12-2010

Predictive Energy Management in Connected Vehicles: Utilizing Route Information Preview for Energy Saving

Chen Zhang
Clemson University, chenz@clemson.edu

Predictive Energy Management in Connected Vehicles: Utilizing Route Information Preview for Energy Saving

---

A Doctoral Dissertation
Presented to
the Graduate School of
Clemson University

In Partial Fulfillment
of the Requirements for the Degree
Doctor of Philosophy
Mechanical Engineering

---

by
Chen Zhang
December 2010

Accepted by:
Dr. Ardalan Vahidi, Committee Chair
Dr. Pierluigi Pisu
Dr. John R. Wagner
Dr. Georges Fadel

Abstract

This dissertation formulates algorithms that use preview information of road terrain and traffic flow for reducing energy use and emissions of modern vehicles with conventional or hybrid powertrains. Energy crisis, long term energy deficit, and more restrictive environmental protection policies require developing more efficient and cleaner vehicle powertrain systems. An alternative to making advanced technology engines or electrifying the vehicle powertrain is utilizing ambient terrain and traffic information in the energy management of vehicles, a topic which has not been emphasized in the past. Today's advances in vehicular telematics and advances in GIS (Geographic Information System), GPS (Global Positioning Systems), ITS (Intelligent Transportation Systems), V2V (Vehicle to Vehicle) communication, and VII (Vehicle Infrastructure Integration) create more opportunities for predicting a vehicle's trip information with details such as the future road grade, the distance to the destination, speed constraints imposed by the traffic flow, which all can be utilized for better vehicle energy management. Optimal or near optimal decision-making based on this available information requires optimal control methods, whose fundamental theories were well studied in the past but are not directly applicable due to the complexity of real problems and uncertainty in the available preview information.

This dissertation proposes the use of optimal control theories and tools including Pontryagin minimum principle, Dynamic Programming (DP) which is a numerical realization of Bellman's principle of optimality, and Model Predictive Control (MPC) in the optimization-based control of hybrid electric vehicles (HEVs), plug-in hybrid electric vehicles (PHEVs), and conventional vehicles based on preview of future route information. The dissertation includes three parts introduced as follows:

First, the energy saving benefit in HEV energy management by previewing future terrain information and applying optimal control methods is explored. The potential gain in fuel economy

is evaluated, if road grade information is integrated in energy management of hybrid vehicles. Real-world road geometry information is taken into account in power management decisions by using both Dynamic Programming (DP) and a standard Equivalent Consumption Minimization Strategy (ECMS), derived using Pontryagin minimum principle.

Secondly, the contribution of different levels of preview to energy management of plug-in hybrid vehicles (PHEVs) is studied. The gains to fuel economy of plug-in hybrid vehicles with availability of velocity and terrain preview and knowledge of distance to the next charging station are investigated. Access to future driving information is classified into full, partial, or no future information and energy management strategies for real-time implementation with partial future preview are proposed. ECMS as well as Dynamic Programming (DP) is systematically utilized to handle the resulting optimal control problems with different levels of preview.

We also study the benefit of future traffic flow information preview in improving the fuel economy of conventional vehicles by predictive control methods. According to the time-scale of the preview information and its importance to the driver, the energy optimization problem is decomposed into different levels. In the microscopic level, a model predictive controller as well as a car following model is employed for predictive adaptive cruise control by stochastically forecasting the driving behavior of the lead car. In the macroscopic level, we propose to incorporate the estimated macroscopic future traffic flow information and optimize the cost-to-go by utilizing a two-dimension Dynamic Programming (2D-DP). The algorithm yields the optimal trip velocity as the reference velocity for the driver or a low level controller to follow.

Through the study, we show that energy use and emissions can be reduced considerably by using preview route information. The methodologies discussed in this dissertation provide an alternative mean for the automotive industry to develop more efficient and environmentally friendly vehicles by relying mostly on software and information and with minimal hardware investments.

Dedication

I dedicate this achievement to my parents, my grandfather, my brother, and all the friends who once helped me during my Ph.D studies in Clemson, SC.

Acknowledgments

First of all, I would like to thank my advisor Dr. Ardalan Vahidi for his kind help, support, and instruction in my Ph.D studies at Clemson University. As he dedicated his energies in research, education and supervision, he was a professional example for his students to study from and to follow. During the last three and half years, under his persistent help and supervision, I was trained from the preliminary to the concluding level and gained professional experience in efficient communication, accurate idea organization, and positive thinking. This resulted in not only the fulfillment of this dissertation but also a supplement to the formation of my personality for future career development. I would like to specially thank Dr. Vahidi for his detailed focus on the careful revision and proofreading of the drafts of this dissertation and several conference and journal publications related to this dissertation. Overall, my experience in Dr. Vahidi's team was friendly, enjoyable, and constructive.

I would like to take this opportunity to thank several members in Dr. Vahidi's research team including Ali Borhan, Grant Mahler, Seneca Schepmann, and Behrang Asadi. The discussion with Ali Borhan brought about the theoretical basis for parts of this dissertation. I would like to thank Grant Mahler for his help in collecting the GPS experimental data and also to thank him for instructing some English writing skills. Seneca Schepmann and Behrang Asadi helped discuss my research and for that I thank them.

Additionally, I wish to thank my committee members, Dr. Pisu, Dr. Wagner, and Dr. Fadel for their comments and encouragements for my research work.

Lastly, I offer my gratitude and regards to all the friends who supported, helped, and encouraged me in any respect during the completion of this dissertation.

Table of Contents

List of Tables

List of Figures

Chapter 1

Introduction

1.1 Background and Motivation

The continuing increase of energy use worldwide, limited resources of fossil energy, and more restrictive environmental protection policies have pushed the industry towards developing more efficient and cleaner energy production. According to the statistical data from U.S. Department of Energy (DOE) [16], the transportation sector accounts for 28% of all the energy use after the industrial sector with 33%, from which 71% comes from petroleum. Improving the fuel economy of fleet of millions of vehicles in the United States, not only has economical and societal impacts but also is strategically important. Corresponding to the large proportion of energy use, emissions contributed by our transportation system dominate all the emission sources and also are gradually growing [72]. A recent proposal by U.S. DOE and EPA (Environmental Protection Agency) [17] requires an increase in fuel economy of vehicles to an average of 34.1 miles per gallon (MPG) by 2016; and an average of 5% improvement annually starting from the vehicle models of 2011. Accordingly, the average green house CO_2 emission requires an average reduction to $250g/km$. Another proposal from National Highway Traffic Safety Administration suggests to raise Corporate Average Fuel Economy (CAFE) requirements to somewhere between 47 and 62 MPG by 2025 [52]. Challenges exist to improve the current vehicle to meet the stringent government policies in fuel economy and emissions.

To respond to these requirements, the automotive industry has focused heavily on the development of more efficient and cleaner vehicle powertrain technologies. Advanced combustion tech-

nologies such as Fuel Stratified Injection(FSI), Homogeneous Charge Compression Ignition (HCCI), Selective Catalytic Reduction (SCR), are among the main approaches toward greener and more efficient vehicle powertrains. The opportunity also exists by reducing the weight of vehicles considering the strong relationship between vehicle weight and fuel consumption. According to a report [30] issued by Ricardo® [1], the average fuel economy will be increased up to 0.65% with every 1% weight loss for passenger vehicles. Another trend is electrifying the vehicle propulsion system relying on new types of energy storage devices such as batteries and supercapacitors or by using fuel cells as the main propulsion source. However, purely electric propulsion is not a mature technology yet due to its higher cost, reliability, and performance limitations. For example, the energy density of a battery is just around 1.5% of the diesel fuel which limits its application. Therefore, hybrid powertrains integrating conventional engines, powertrains, and auxiliary energy storage devices have drawn more attention in recent years. The most popular hybrid powertrain system currently is the hybrid of a combustion engine and batteries, as the electrochemical battery industry develops rapidly. A hybrid powertrain usually has a smaller engine but runs more efficiently; it has the capability to partially recuperate the braking energy, which is usually wasted as heat, and increase the vehicle efficiency significantly at the partial load condition e.g. at low speeds. Consequently, the fuel economy of a hybrid vehicle is much better than a vehicle with a conventional powertrain. Toyota Prius, the most successful commercialized HEV model with an average fuel economy up to 50MPG and sales volume more than 1.2 million, visualizes the potential of the HEV powertrain for reducing fuel use and emissions in next decades.

An almost untapped approach for reducing the energy consumption of ground vehicles is using various information sources and by predictive motion planning. Consider the following three examples in which lack of information about future events down the road can negatively influence the fuel economy of a vehicle:

1. A hybrid electric vehicle (HEV) reaching the top of a hill with a fully charged battery pack is unable to capture the free braking energy that is available on the steep downhill descent. This is due to the unknown future terrain.

2. A plug-in hybrid electric vehicle (PHEV) that depletes its charge before arriving at the destination is not utilizing energy optimally. The optimal solution is to discharge the battery

[1] Ricardo® is a registered trademark of Ricardo INC.

gradually so the battery is depleted at the charging destination. This is due to unknown trip distance.

3. A vehicle's untimely arrival at a local traffic wave with lots of stops and goes will increase the use of fuel and wears the engine and friction brakes. This is due to unknown future traffic flow.

These examples illustrate some instances in which use of information and preview can enhance the energy utilization in a vehicle. Due to dependence on advanced telematics and wireless connectivity, the value such preview information can have in improving the fuel economy of vehicles has not been widely explored in the past. Even when available, telematics information has been used only in other areas: more specifically, previewing traffic information has shown its value in advanced traveler information systems (ATIS), advanced transportation management systems (ATMS)[48], and active safety systems [58, 12]. For example, ATIS can help travelers in making better route choices to save traveling time and avoid traffic jams; ATMS traffic preview can be used for assigning optimal dynamic speed limits in controlling the traffic of a highway entrance, and in properly timing traffic signals; a vehicle with anticipation of traffic-signal violation, curve-speed warning, and emergency electronic brake lights [12] can avoid the violation and collision.

Recent advances in traffic information technology via Geographic Information Systems (GIS), Global Positioning System (GPS), Intelligent Transportation Systems (ITS),Vehicle to Vehicle (V2V) communication present more opportunities for predicting the vehicle trip information with details such as the future road grade, the remaining distance to destination, and the speed constraints imposed by the traffic flow. For instance a vehicle, localized by in-vehicle GPS is able to identify its future route topology by integrating in-vehicle 3D road maps containing the altitude, longitude, and altitude information of the road.

Predicting the traffic condition surrounding a vehicles is more challenging due to dynamically changing nature of traffic but can have great value in motion planning of vehicles for fuel saving. Interestingly preview of traffic flow information is potentially attainable today with existing real-time traffic databases and advanced traffic prediction methods. Real traffic data could be retrieved from local traffic channels, GPS-enabled vehicle navigation systems, cellular phone networks, or short range communication with surrounding vehicles. Google, for example, currently streams real-time traffic information of major U.S. cities and includes an estimate of average speed of vehicles in each

road segment (see the latest edition of Google Earth and its traffic layer.). Another example is the statewide sensor systems in California which consist of 25,000 sensors located on mainlines and ramps, and grouped into 8,000 vehicle detector stations (VDS) to monitor in real-time the state of traffic [46]. Because of the high maintenance cost and not so widespread distribution of the sensor networks on roads, there has been growing interest in using individual vehicles as moving probes for estimating the state of traffic. This trend was demonstrated by a cooperative project between University of California at Berkeley and Nokia in a project called "Mobile Millennium" since Nov. 2008 [2] aiming at gaining real time traffic information from mobile phones inside each participating vehicle. Also the concept of connected or networked vehicles has been visualized as a next generation vehicle technology and a test facility for it has been constructed in Michigan International Speedway in 2009 [1]. In the connected vehicle vision, the vehicles can communicate with each other wirelessly and share driving information with surrounding vehicles enabling cooperative driving. With current technology, the frequency of wireless transmission varies from 1 Hz to 50 Hz, while the desired communication range varies from 50 m to 300 m [12].

Given these various sources of real-time traffic information, predicting the state of traffic over a future time horizon can now be done more reliably than before. Prediction of traffic flow could be either simulation-based or statistical based. The former uses traffic models and interaction of vehicles within traffic network to project the state of future traffic while the latter uses historic traffic data. Combining the simulation based and statistics based methods yields a hybrid method that has the strengths of both approaches [48]. Most uses of such information have been for navigation and routing purposes using mostly ad-hoc or proprietary routines. An untapped opportunity lies in utilizing this vast source of dynamic information for better energy management of conventional vehicles. For conventional vehicles preview can help plan an eco-friendly speed profile which saves fuel and reduces emissions without increasing trip time. This eco-friendly speed can be suggested to the driver or directly incorporated in vehicle's adaptive cruise control module.

1.2 Thesis Overview

In this thesis, we propose systematic utilization of optimal control methods including Pontryagin minimum principle, Bellman's principle of optimality and Model Predictive Control(MPC) with different types of preview information such as terrain information, trip distance, traffic flow

information in three areas of vehicle technology, namely in hybrid electric vehicle (HEV), plug-in hybrid electric vehicle (PHEV) and conventional vehicle powertrain systems to improve their energy utilization. We focus our study on reducing energy consumption as well as emission.

For HEV and PHEV studies, the goal is to quantify reductions in energy usage attainable by using preview information of road terrain, traffic speed, and length of a trip. The minimum-energy-use benchmark for this study is calculated by solving the energy minimization problem via Dynamic Programming (DP) assuming access to full future information. Then we consider more realistic cases where only partial preview is available. Equivalent Fuel Consumption Minimization Strategy (ECMS), a variation of Pontryagin minimum principle is emphasized for HEV and PHEV optimal control in which its parameters are estimated based on different types of future driving information. This part of the work is presented in chapter 2 (Role of Terrain Preview in Energy Management of Hybrid Electric Vehicles) and chapter 3 (Route Preview in Energy Management of Plug-in Hybrid Electric Vehicles).

Specifically, in chapter 2, we quantify the potentials of 3D road terrain maps for improving the fuel economy of a parallel hybrid vehicle. In this study, we decouple the influence of velocity variation by focusing on constant-velocity cruise situations. The future road terrain can be determined using in-vehicle 3D maps and the vehicle GPS-based navigation. In this work we use real world 3D aerial maps created by Intermap Technologies. The digital elevation maps and orthorectified radar images are gathered using a proprietary airborne Interferometric Synthetic Aperture Radar (IFSAR) technology from a fixed-wing aircraft. With availability of future driving condition, the optimal control methods DP and ECMS are proposed and compared against two baselines without any future preview.

Chapter 3 investigates the gains in fuel economy attainable by information preview for plug-in hybrid electric vehicles. Our study classifies four different levels of access to future information for power management of a PHEV: i) full knowledge of distance, future velocity, and upcoming terrain profile, ii) full knowledge of upcoming terrain and estimated velocity from historic traffic data or real-time traffic data streams, iii) knowledge of distance to the next charging station, iv) no future information. Different control strategies are proposed for different levels of preview. With full knowledge of future driving conditions, DP is performed to obtain a benchmark for the best achievable fuel economy. ECMS is proposed as an instantaneous optimization strategy with its co-state parameter tuned based on preview. Parameter estimation methods corresponding to different

preview levels are then developed. The proposed method are tested through several case studies with federal standard driving cycles and real driving cycles.

Chapter 4 investigates the benefit of future traffic flow information preview in improving the fuel economy of conventional vehicles by predictive control methods. According to the time scale of traffic events, the energy optimization problem is decomposed into different levels. At a microscopic level, a model predictive controller as well as a car following model is integrated for predictive adaptive cruise control by stochastically forecasting the driving behavior of the lead car. The distribution of the lead car position is approximately calculated using a Markov chain Monte Carlo (MCMC) simulation. A corresponding stochastic model predictive control problem is then converted to a deterministic model predictive control for which efficient real-time solutions exist. At a macroscopic level, we propose to incorporate the estimated macroscopic future traffic flow information based on gas-kinetic traffic models and optimize the cost-to-go by utilizing a two-dimension Dynamic Programming (2D-DP). The solution yields the optimal trip velocity as the reference velocity for the driver or a low level vehicle controller. Different case studies shown demonstrate the value of previewing traffic evolution in reducing the energy consumption of a vehicle.

Chapter 2

Role of Terrain Preview in Energy Management of Hybrid Electric Vehicles

2.1 Introduction

Today's hybrid electric vehicles (HEV) have much better fuel economy than the conventional non-hybrid vehicles. The improved fuel economy is mainly due to use of extra battery energy storage and one or more electric machine which assist the combustion engine by providing additional power, and therefore allow use of a smaller combustion engine operating in its more fuel efficient conditions. The battery storage also provides a buffer which enables capturing the braking energy that is normally wasted as heat. The extra degree of freedom provided by the auxiliary power source enables substantial improvements in fuel efficiency as demonstrated by the commercially available hybrid electric vehicles. Yet the added efficiency of any HEV is dependent on the power management strategy (PMS) which determines the split of power request between the combustion engine and electric drive [66].

Most power management strategies in production vehicles operate based on logical "if-then-else" type rules and pre-optimized maps and rely only on instantaneous power demand and state of the vehicle [9, 74, 11, 22]. In search of an optimal (or sub-optimal) solution, many researchers have

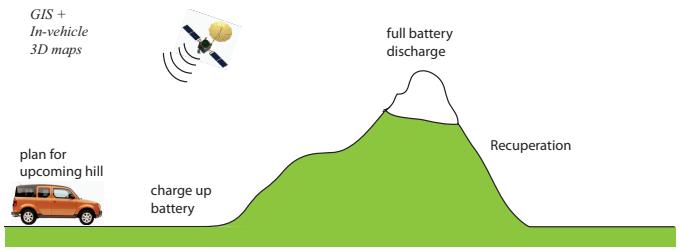

Figure 2.1: Schematic of predictive energy management based on 3D terrain maps.

formulated the PMS as a fuel minimization problem over a driving cycle.

This optimal control problem can be solved by numerical Dynamic Programming (DP) assuming full or statistical knowledge of the future driving cycle [43, 32]. Because of its dependence on future driving cycle and its large computational burden, DP is not suitable for online use and considered only as a benchmark for best achievable fuel economy [43]. Instead to obtain a sub-optimal solution, the global optimization problem is simplified to an instantaneous one in the family of ECMS (Equivalent Consumption Minimization Strategy) methods [37, 53, 60, 65]. In the ECMS methods, the battery charging/discharging at each instant is translated to equivalent fuel gained/used and the sum of instantaneous actual and equivalent fueling rate is minimized. ECMS methods are computationally efficient, however their performance may vary depending on the cycle because of lack of information about upcoming driving cycle.

The truly optimal power management strategy depends on the future driving conditions. Knowledge of upcoming terrain and traffic conditions will help more judicious use of the electric power by extending the planning horizon. Such information can now become available as illustrated in Fig. 2.1 by combined use of vehicle navigation system, 3D road maps, and even possibly radioed traffic information. Research has been done in the past on use of preview road information for improving fuel economy of commercial heavy trucks with conventional powertrains [29]. Look-ahead use of traffic and traffic signal information has been proposed as a mean to predict future velocity profile [19] or reduce rapid accelerations and decelerations which helps the fuel economy [3, 36] . While there is the belief among HEV experts that preview terrain information can increase the fuel efficiency of hybrid vehicles, the amount of possible improvement to fuel economy has not been clearly explored in the literature [63, 32], nor is there a systematic methodology to utilize such preview knowledge in the existing power management strategies. The adaptive ECMS (A-ECMS) [60] and telemetry ECMS (T-ECMS) [64] power management algorithms aim to respectively use

the past and partial future information to adjust their tuning parameter. However none explores knowledge of future terrain information.

In contrast to the past research, the main purpose of this part is to quantify the potentials of 3D road terrain maps for improving the fuel economy of a parallel hybrid vehicle. In the present study, we decouple the influence of velocity variation by focusing on constant-velocity cruise situations. The future road terrain can be determined using in-vehicle 3D maps and the vehicle GPS-based navigation. In this work we use real world 3D aerial maps created by Intermap Technologies. The digital elevation maps and orthorectified radar images are gathered using a proprietary airborne Interferometric Synthetic Aperture Radar (IFSAR) technology from a fixed-wing aircraft.

Section 2.2 presents the vehicle configuration and its model for simulation. Section 2.3 summarizes seven road terrain profiles, three of which are simulated arc terrains and the other four are real terrain profiles from California mountain area. In Section 2.4, the energy management strategies with and without preview are presented. Section 2.5 evaluates the impact of terrain preview on fuel economy based on several simulation results. Section 2.6 concludes this part with a summary of our observations.

2.2 The HEV Powertrain Configuration and Model

A midsize 2000kg passenger vehicle with a parallel hybrid electric configuration is selected for this study. Parameter values and detailed performance maps for various powertrain components were extracted from the database of Powertrain System Analysis Toolkit (PSAT) simulation software developed by Argonne National Laboratory [40]. A 120kW gasoline internal combustion engine and a 45kW AC motor are arranged in a pre-transmission configuration and connected to a 5 speed automatic transmission via a clutch and a torque coupler. The key vehicle parameters are summarized in Table 3.1.

Table 2.1: Specification of a parallel HEV for simulation

maximum engine power	120kw	maximum motor power	45kw
battery capacity C	5.5 Ah	battery voltage	312V
reducer ratio	2	final drive ratio	10.5

The PSAT-based full-order powertrain model contains the vehicle velocity, the clutch input speed, and battery state-of-charge (SOC) as its dynamic states with many other look-up tables and logical switches. Maintaining this level of complexity for developing and evaluating an optimal

power management scheme is neither practical nor necessary. In fact, the only state critical in power management is the slowly varying state of charge of the battery [66]. Therefore a reduced-order model is developed which contains the battery state of charge as its only dynamic state. The battery is modeled with its open-circuit voltage in series with a constant internal resistance. State-of-charge (SOC) dynamics are described by:

$$\frac{d}{dt}SOC = -\frac{V_{oc} - \sqrt{V_{oc}^2 - 4P_{batt}R}}{2RC} \tag{2.1}$$

where V_{oc} is the open circuit voltage of the battery, P_{batt} is the electric power at battery output side, R is the internal resistance of the battery and connecting wires, and C is the battery capacitance. More details can be found in [61]. In the reduced-order model we continue to use look-up tables from PSAT to model the engine fuel rate and motor losses. The fuel rate $\dot{m}_f$ is mapped from the engine torque T_{eng} and engine speed ω_{eng}:

$$\dot{m}_f = f(T_{eng}, \omega_{eng}); \tag{2.2}$$

Another look-up table is used to relate the motor mechanical power P_m to motor speed ω_m and output electrical power of the battery P_{batt},

$$P_{batt} = g(P_m, \omega_m); \tag{2.3}$$

The gear shifting strategy, which depends on wheel torque demand and vehicle velocity, is also adopted from PSAT and implemented as a lookup map.

2.3 The Test Road Profiles

Two sets of road elevation profiles are used for this study. The first is a set of three simulated arc terrains with the same span, but different peak elevations, and maximum grades; Figure 4.4 shows their profiles. The second is a set of four real world road profiles selected from Intermap's 3D terrain map database. Figure 2.3 shows a Google Map®[1] of this region in Contra Costa county in California. Intermap's road geometry database has the information stored as 3D road vectors with accurate longitude, latitude, and altitude. This information is post-processed and converted to 2D

[1]Google Maps® is a registered trademark of Google INC.

information in which slope is a function of distance along the road. Figure 2.4 shows the elevation profile for each of these roads. The statistical information of the grades including maximum and minimum road slope and the slope root-mean-square (RMS) values are listed in Table 2.2.

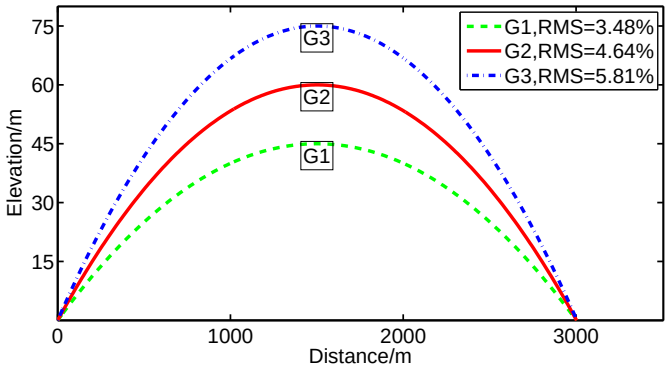

Figure 2.2: Simulated arc terrain elevation profiles G1-G3 and their root-mean-square grade values.

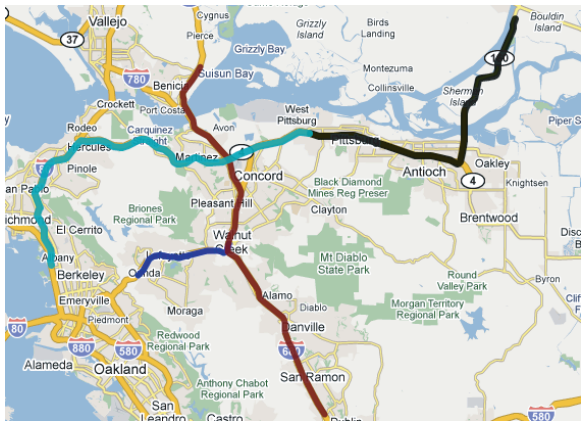

Figure 2.3: A Google map view of terrain G4-G7 in Contra Costa county, CA.

Table 2.2: Statistics of the terrain data

route	length(km)	mean(%)	max(%)	min (%)	RMS (%)
G4	12	0.77	4.02	-3.73	2.1877
G5	48	0.26	4.72	-3.73	1.32
G6	36	-0.21	2.96	-4.33	1.04
G7	48	-0.17	5.32	-7.97	2.31

In this discussion the focus is on realizing the fuel economy gains with road grade preview only. To decouple the influence of unknown future velocity, we assume that the vehicle is traveling with a constant and known cruise speed. The case with varying speed requires further investigation and is planned as a next step of this work. With the known speed assumption, upcoming slopes will be known as a function of time.

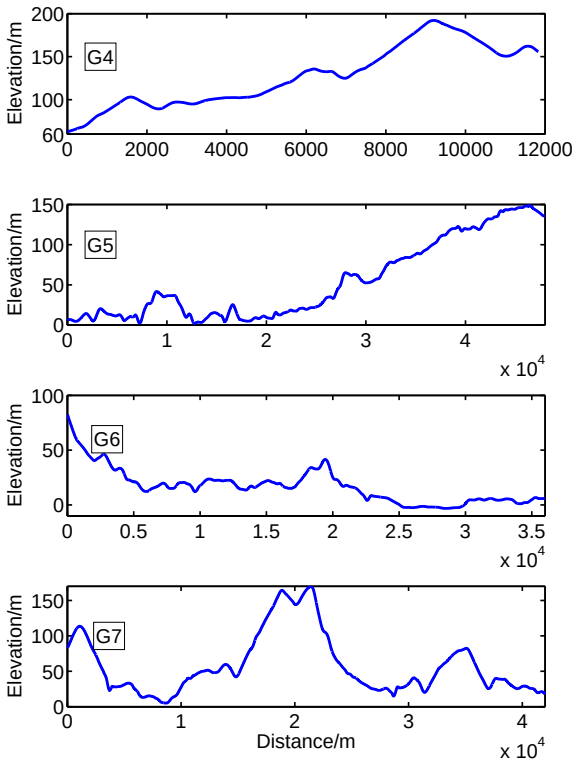

Figure 2.4: Elevation profiles of real world terrains G4-G7

2.4 Power Management Strategy

The supervisory control unit of an HEV determines the power or torque split ratio between the combustion engine and the electric motor aiming to reduce fuel use. This section describes the structure of two types of power management strategies (PMS) used in this work: i) strategies which determine the baseline achievable fuel economy without terrain preview and ii) strategies with terrain preview. Finding a "fair" baseline PMS, i.e. one that is near-optimal in absence of preview, was one of the main challenges of this research. We have considered both a rule-based and a modified ECMS method as baseline strategies without preview. When terrain preview is available, we use both ECMS and dynamic programming to determine the best achievable fuel economy. The details of each algorithm is described next.

2.4.1 Rule-Based Control Strategy

A rule-based power management scheme is considered first, because such rule-based strategies are most widely used in current hybrid vehicles. Examples of different rule-based strategies can

be found in research papers as well [43, 22, 57]. We adopt the structure of the rule-based strategy used in PSAT which could achieve good fuel economies for most tested cycles. To increase the fuel economy, the rules are designed to turn off the engine at low power demands and run it near statically optimized operating lines when on.

In this rule-based strategy, the desired charging or discharging power of the battery, P_{batt_dmd} is calculated as a static function of the battery's state of charge, SOC. A positive P_{batt_dmd} denotes charging and a negative value means discharging power. The driver's power request P_{drv_dmd} is inferred from the accelerator pedal position (or through a driver model in simulations). The sum of the driver and battery power demands determines the total power demand P_{dmd},

$$P_{dmd} = P_{drv\_dmd} + P_{batt\_dmd} \tag{2.4}$$

from which the total torque demand T_{dmd} at the torque coupler is calculated by dividing the known engine speed[2]. A statically optimized map is used along with a set of rules to determine the engine and motor torques. Figure 2.5 shows a schematic of this map partitioned into 5 different regions by statically optimized curves. In this figure the *normal optimal curve* (T_{opt}) represents the most efficient operating line of the engine as a function of the engine speed. However operating the engine on this line does not necessarily result in minimum fuel use. In other words running the engine most efficiently is not always equivalent to running the hybrid powertrain most efficiently. This is due to electrical losses that needs to be accounted for in the calculation of engine best operating points. In the rule-based approach, two additional curves the *high optimal curve* (T_{opt_hi}) and the *low optimal curve* (T_{opt_lo}) are also calculated which allow operating the engine higher or lower such that overall efficiency is increased. The following rules are used,

- At very low torque levels when (ω_{eng}, T_{dmd}) is in region A, running the engine is not efficient; the engine is turned off (T_{eng}=0) and the motor drives (brakes) the vehicle ($T_{mot} = T_{dmd}$).
- When (ω_{eng}, T_{dmd}) is in region B, the engine is run on the low optimal line ($T_{eng} = T_{opt\_lo}$) and the excess torque is used to charge the battery, i.e. ($T_{mot} = T_{dmd} - T_{opt\_lo}$).
- When (ω_{eng}, T_{dmd}) is in region C, the engine is run on the normal optimal line ($T_{eng} = T_{opt}$) and ($T_{mot} = T_{dmd} - T_{opt\_hi}$).

[2]The vehicle speed is known, the transmission status is also external to the rule-based controller and known and therefore engine speed can be calculated.

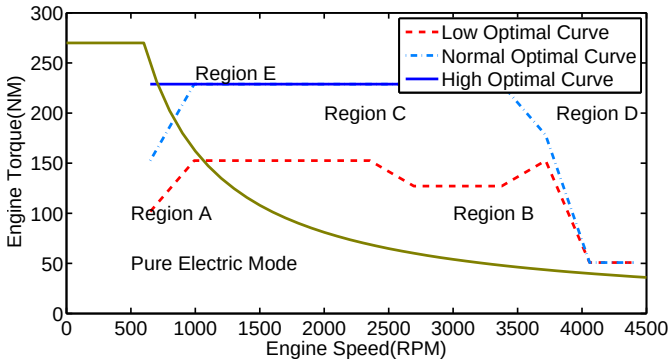

Figure 2.5: Schematic of different operating regions imposed by a rule-based power management strategy

- When (ω_{eng}, T_{dmd}) is in region D, the engine is run on the high optimal line $(T_{eng} = T_{opt\_hi})$ and $(T_{mot} = T_{dmd} - T_{opt\_hi})$.
- At very high torque levels when (ω_{eng}, T_{dmd}) is in region E the engine cannot meet the torque demand, the engine is run on the high optimal line $(T_{eng} = T_{opt\_hi})$ and the motor supplies the rest $(T_{mot} = T_{dmd} - T_{opt\_hi})$.

Since it is difficult to systematically incorporate future information in the rule-based strategy, it is only treated as a baseline strategy without preview.

2.4.2 Optimal Control Strategy-ECMS

Maximizing fuel economy of an HEV can be explicitly formulated as minimization of the cost function [22]:

$$J_f = \int_{t_0}^{t_f} \dot{m}_f(t,u)dt + \phi(SOC_i, SOC_f); \tag{2.5}$$

subject to the powertrain model equations and the following constraints:

$$\begin{aligned} SOC_{min} \leq SOC \leq SOC_{max} \\ T_{eng}^{min}(\omega_{eng}) \leq T_{eng}(\omega_{eng}) \leq T_{eng}^{max}(\omega_{eng}) \\ T_{m}^{min}(\omega_{m}) \leq T_{m}(\omega_{m}) \leq T_{m}^{max}(\omega_{m}) \end{aligned} \tag{2.6}$$

where $\dot{m}_f$ is the fuel consumption rate; the control law u is the power split ratio; SOC_i and SOC_f are the initial SOC and final SOC respectively; SOC_{min} and SOC_{max} are the minimum and maximum

bounds on SOC; $T_{eng}^{min}(\omega_{eng})$ and $T_{eng}^{max}(\omega_{eng})$ are the minimum and maximum torque of the engine at given speed; $T_m^{min}(\omega_m)$ and $T_m^{max}(\omega_m)$ are the minimum and maximum torque of the electric motor at given speed; $\phi(SOC_i,\ SOC_f)$ is the penalty function (also referred as equivalent fuel consumption) for the deviation of final SOC from its initial value. The final SOC is usually constrained to be equal to the initial SOC; in that case $\phi(SOC_i, SOC_f)$ will vanish.

Analytical solutions to this optimization problem do not exist in general, due to its many state and input constraints, nonlinearities, and its dependence on future power demands.

In the Equivalent Fuel Consumption Minimization Strategy (ECMS) the above optimization problem is simplified to minimization of the *instantaneous* (rather than integral) equivalent fuel rate $\dot{m}_{f,equ}$ as shown in Eq. 3.6 [57]:

$$\dot{m}_{f,equ} = \dot{m}_f + s \cdot P_e / H_l \tag{2.7}$$

where P_e is the net power charged to the battery or the power drawn including the power loss to the internal resistance; H_l is the lower heating value of the fuel.

2.4.2.1 ECMS Without Preview

Choice of the fuel equivalence factor s is important and critical to fuel economy and charge sustenance of the battery. Its true value is a function of future power demands which are unknown in absence of preview. Several methods were proposed to estimate s [37, 65, 60]. In [22] average charging and discharging efficiencies are used to approximate the value of s as follows:

$$s = \begin{cases} s_{dis} & P_e(t,u) > 0 \\ \\ s_{chg} & P_e(t,u) < 0 \end{cases}$$

where

$$s_{dis} = \frac{1}{\bar{\eta}_e^{(d)} \bar{\eta}_f} \tag{2.8}$$

$$s_{chg} = \frac{\bar{\eta}_e^{(c)}}{\bar{\eta}_f} \tag{2.9}$$

Here $\bar{\eta}_e^{(d)}$ and $\bar{\eta}_e^{(c)}$ are the average electric circuit efficiencies for discharge and charge respectively; $\bar{\eta}_f$ is the average efficiency for the combustion engine.

Because this choice of s is not a function of the battery's state of charge, the SOC may deviate far from its desired value. Inspired by the approach in [65] in our baseline ECMS we modify s as a function of SOC based on the bilinear relationship shown in Figure 2.6. The values of s_{chg} and s_{dis} are determined using Equations (2.8) and (2.9) based on assumed average efficiencies and without using preview.

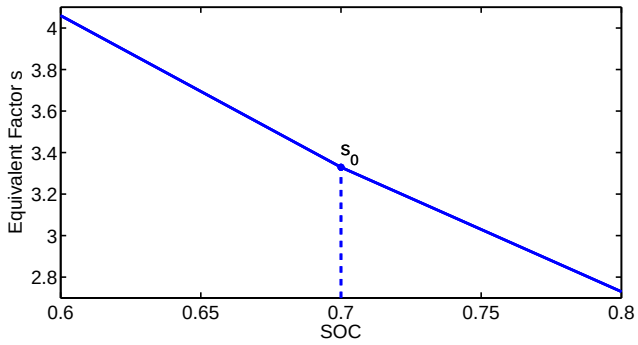

Figure 2.6: Equivalent factor s as function of SOC; $s_0 = \sqrt{s_{dis} s_{chg}}$.

Also we enforce the following additional rules to ensure that the SOC does not exceed its limits:

- If $SOC > SOC_{max}$, charge mode is not allowed.
- If $SOC < SOC_{min}$, discharge mode is not allowed.

SOC_{max} and SOC_{min} are set to 0.8 and 0.6 respectively in our study which is consistent with bounds enforced in practice.

2.4.2.2 ECMS with Preview

With known future power demands, it is possible to find the true value for the equivalence factor s. It is shown that the value of s that results in minimum fuel use and renders $SOC_f = SOC_0$ is a constant [14] if,

- the SOC constraint in (2.6) is relaxed and
- if the right-hand side of SOC dynamics (2.1) is not an explicit function of SOC.

– The open circuit voltage V_{oc} and internal resistance R are constants.

The details of the derivation can also be referred in Section 3.4.1.2. We use a numerical procedure that iterates to find the constant value of s with known future power demands at the beginning of each driving cycle. Specifically, in this process, a constant s is guessed initially and the optimization is carried out based on this initial value of s. The resulting final state of charge SOC_f is then compared to the desired value SOC_0. If different, the value of s is updated based on a bisectional search and the process is repeated till finally $SOC_f = SOC_0$.

2.4.3 Optimal Control Strategy-Dynamic Programming

When the future power demands are known, the optimal power-split ratio that minimizes the cost function (3.2) subject to model equation and constraints in (2.6) can be numerically obtained using dynamic programming [43]. The time-horizon, the state variable SOC, and the control variables are discretized and the optimal control problem is solved backwards in time according to Bellman's principle of optimality. Details of DP can be found in the part 3.3.2.1.

In simulations, we observed little difference between the results of DP and that of ECMS with preview. To see the difference between DP and ECMS with preview, the fuel economies of the two control strategies are compared as shown in Fig. 2.7 for simulated grades G1, G2, and G3 and for the cruise speeds of 30, 45, and 60 mph. It can be seen that in most cases the difference is less that 1 percent and the largest difference is around 2 percent. The difference could be due to linear approximation and discretization errors in DP which may make DP deviate from the true optimal solution. Another potential factor for the difference is that the SOC trajectory in standard ECMS is allowed to go over its constraints while DP enforces the SOC constraints. However, this factor was not the case for simulations in Fig. 2.7.

Therefore, for the sake of reducing computational burden, in the rest of the simulations in this part, standard ECMS is considered as the control strategy with preview unless SOC constraint in ECMS is violated; in that case the DP result will be used.

2.5 Simulation Analysis

To determine the impact of terrain preview on fuel economy, we compare the fuel economy obtained via ECMS with preview (or DP with preview) to that of ECMS and rule-based strategies

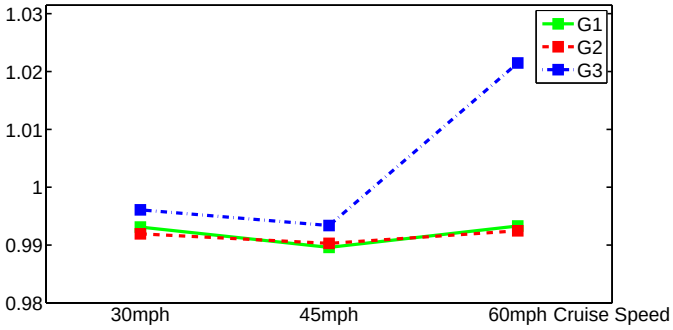

Figure 2.7: Fuel economy gains with DP and ECMS both with terrain preview. The *y axis* shows the ratio between the fuel economies with DP and standard preview ECMS.

without preview. The rule-based strategy without preview is representative of the industry approach and the ECMS without preview has been more an academic approach; therefore both are used as representative "baseline" strategies.

2.5.1 Results with Simulated Terrains G1-G3

The fuel economy improvements with preview obtained with the ECMS or DP methods, are compared to that from baseline control strategies of ECMS and rule-based without preview for three cruise velocities of 30, 45, and 60 mph. The comparisons are illustrated in Fig. 2.8.

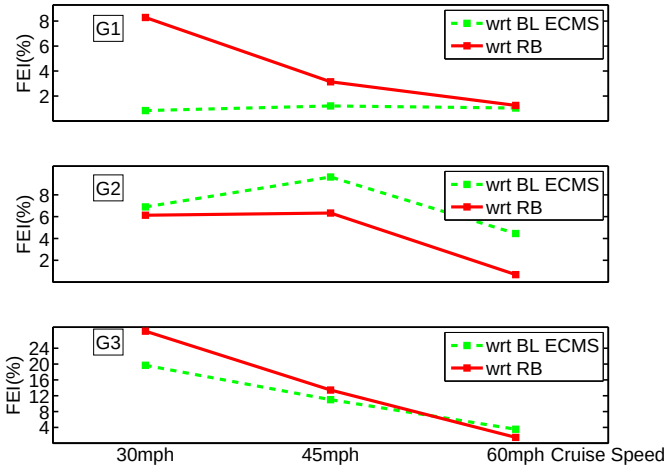

Figure 2.8: Fuel economy improvement (FEI) of arc terrains with respect to (wrt) baseline ECMS (BL ECMS) and rule-based (RB) strategy .

From the simulation, we observe that:

1. When compared to the ECMS baseline, the optimal strategy with preview yields 0.8%-20% improvement in fuel economy. When compared to the rule-based baseline, the improvement can be even higher and as high as 28%. The improvement is higher for G3 which is the steepest profile; in other words when the root-mean-square value of grade is higher, the improvement is more. Large improvement (up to 28%) is obtained in arc terrain G3 during 30 mph cruise because of balancing the buffer of the battery and future free regeneration energy in advance. This is better illustrated in Fig. 2.9 that shows the optimal preview solution obtained via DP is able to leave enough buffer in the battery on the top of the hill in anticipation of future regeneration energy.

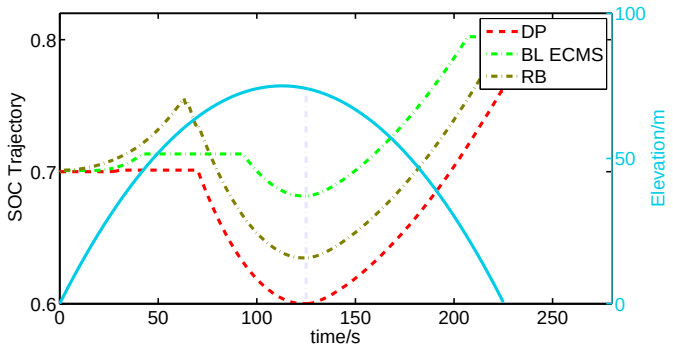

Figure 2.9: Comparison of SOC trajectories for different control strategies with G3 profile and cruise speed 30mph.

2. The results consistently indicate that terrain preview may be more effective at lower speeds. At higher speeds the power demands are higher and therefore less regeneration opportunity is available.

3. For some simulation cases, e.g. G2, the rule-based baseline achieves better fuel economies than baseline ECMS which illustrates that the performance of rule-based control is not uniform for different simulation cases. Rule and parameters optimized for some cases are not necessarily best for others, a fundamental problem of rule-based strategy. Based on the more consistent performance of the baseline ECMS, it is expected that the improvement with respect to baseline ECMS would be less than 2% over arc terrains "flatter" than G1. However, the same can not

be said when the rule-based strategy is used as the baseline.

4. Since an important advantage of terrain preview is better utilization of battery buffer for regeneration, the improvement is expected to decrease as the size of the battery is increased. We examined this by increasing the battery size to 11Ah from original size of 5.5Ah; the results in Fig. 2.10 confirm this expectation. Therefore terrain preview may be an enabler for reducing battery size in HEVs.

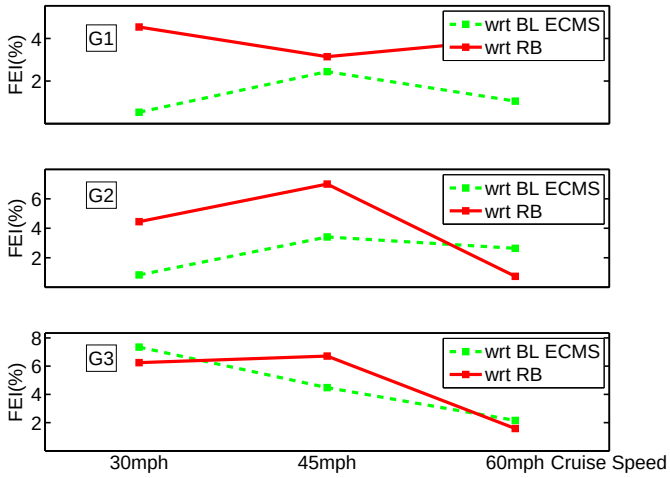

Figure 2.10: Fuel economy improvement (FEI) in arc terrains with respect to (wrt) baseline ECMS (BL ECMS) and rule-based (RB) strategy with a 11 Ah battery.

2.5.2 Results with Simulated Terrains G4-G7

Grades G1-G3 represent a single hill event. To determine the average impact of preview when cruising on rolling terrain, the above process was repeated for real-world terrain profiles G4-G7. The following information is summarized from the simulation results shown in Fig. 2.11:

1. The improvement with respect to baseline ECMS is from 0.07%-6.8% which depends on the grade and velocity. The improvement for G4 and G5 is around or less than 2%. The improvement for G6 and G7 is around 2-3%. The improvement is lower at higher velocities.

2. The improvement with respect to rule-based strategy is between 0.95% and 4.2% depending on the grade and velocity. However, the correlation between improvement and velocity is not

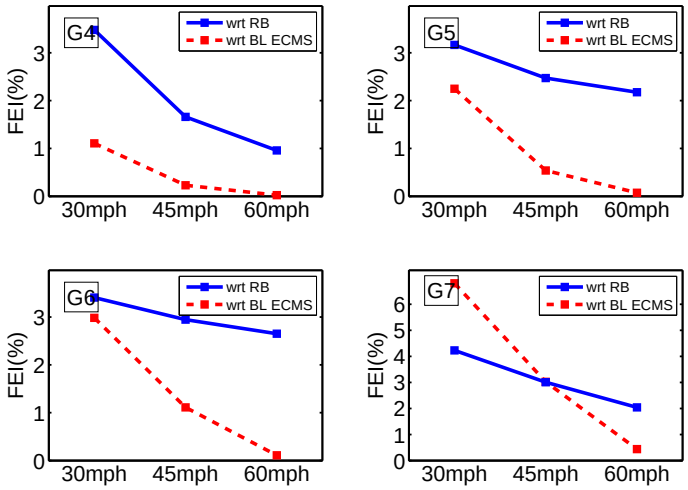

Figure 2.11: Fuel economy improvement (FEI) with respect to (wrt) rule-based (RB) control and baseline ECMS (BL ECMS).

as clear as with baseline ECMS. That means future information may be important for fuel saving even for high speeds when the rule-based strategy is the baseline.

3. In all cases, the improvement at low cruising speed (30mph) is significant and up to 3% or more, which indicates terrain preview may be more useful at low speeds.

4. Preview of long distance downhill or steep grade profiles increases the fuel saving e.g. over terrains G6 and G7. The G6 terrain is a descending terrain resulting in a negative average grade. Preview allows the controller to discharge the battery down and later run the engine at a higher efficiency operating point to charge the battery. G7 features steep spikes in elevation resulting in large maximum, minimum, and root-means-square grades. Over G7, the significant change of elevation over a short interval makes available large regeneration energy that can be better harnessed with availability of terrain preview.

2.5.3 Analysis of Powersplit Behavior with and without Preview

Terrain preview allows more efficient operation of the powertrain by predictive planning and also enables capturing larger portions of future free regeneration energy. This behavior is illustrated in more detail in this section by a few simulation case studies.

Figure 2.12 shows how predictive planning allows recuperating more energy into the battery during downhill descent. Over the G7 terrain and with cruise speed of 30 mph, the DP solution an-

ticipates the future free energy and is able to leave enough buffer which formes the "local minimum" for SOC at hill top points A and B as shown in Fig. 2.12. The correlation between "local minimum" of *SOC* and top point of hill also holds for other points followed by steep downhill grade e.g. point A'. This kind of correlation becomes weak, disappears, or even reverses depending on the steepness of the grade and driver's power demand. An inverse correlation example could be seen from point B' where the local top point of hill does not correlate with "local minimum" but "local maximum" value of *SOC*. More examples and explanation for the "inverse correlation" are shown in Fig. 2.16.

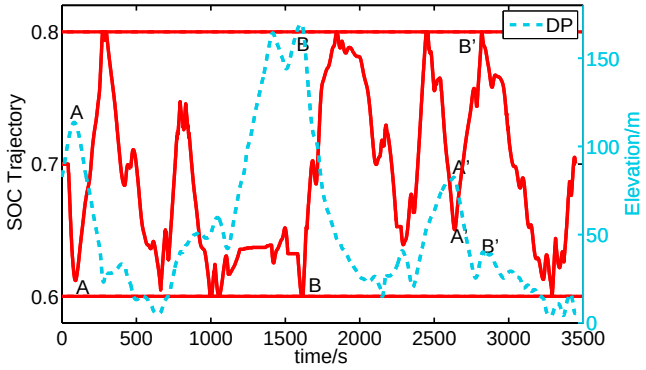

Figure 2.12: SOC trajectory of DP for G7 terrain with cruise speed of 30 mph. The solid and dashed lines show the SOC trajectory and road elevation respectively.

Baseline ECMS and rule-based strategy are unable to capture part of available regeneration energy because of lack of future information. In Figure 2.13, SOC trajectories for baseline ECMS and rule-based are flat at the hill bottom points C and D due to hitting SOC's upper bound.

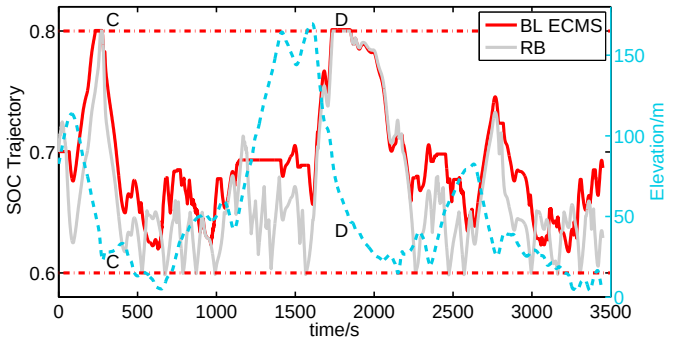

Figure 2.13: SOC trajectories of baseline ECMS (BL ECMS) and rule-based (RB) strategy for G7 terrain and cruise speed of 30 mph. The solid and dashed lines show the SOC trajectory and road elevation respectively.

The engine operating point is also critical for fuel saving. Figures 2.14 and 2.15 show the

engine operating point in speed-torque and torque-time planes respectively for G6 terrain and cruise speed of 30 mph and with DP, baseline ECMS, and baseline rule-based strategies.

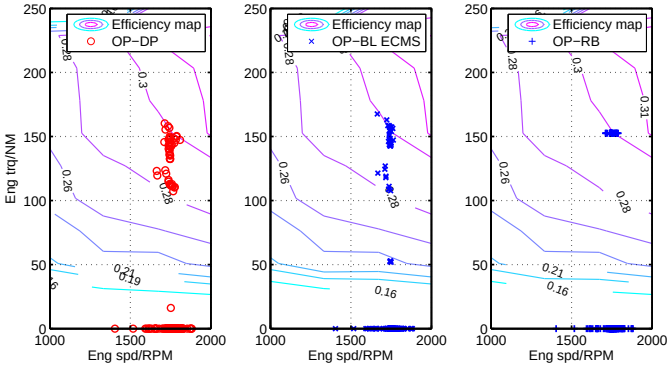

Figure 2.14: Engine operating point (OP) of different control strategies (DP, BL ECMS and RB) with the G6 terrain and 30 mph cruise.

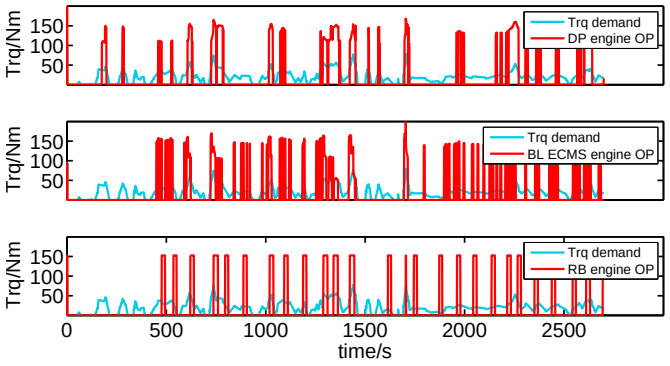

Figure 2.15: Time domain engine operating point (OP) of different control strategies (DP, BL ECMS and RB) in the case with grade G6 and cruise speed 30mph.

In the torque-speed plane, we observe that DP with preview and baseline ECMS and rule-based strategies without preview all manage to operate the engine near efficient operating points when the engine is on. The main differences between them are seen in Figure 2.15 in the engine on/off timing. Due to lack of preview, baseline ECMS and rule-based strategy turn the engine on and off as a function of instantaneous battery state of charge. In the lengthy downhill case of G6 terrain, the engine is turned on less frequently and the battery is depleted to its lower bound as shown in Figure 2.16. With preview, the DP acts more predictively and charges the battery in short uphill intervals $E - F$ and $G - H$ where due to higher torque demands running the engine is more efficient. This results in better fuel economy of the DP approach. We note that this behavior on

G6 is different from that on G7 shown earlier where going uphill, DP would discharge the battery. These decisions are highly dependent on the type of terrain and the optimal power split sometimes is not intuitive.

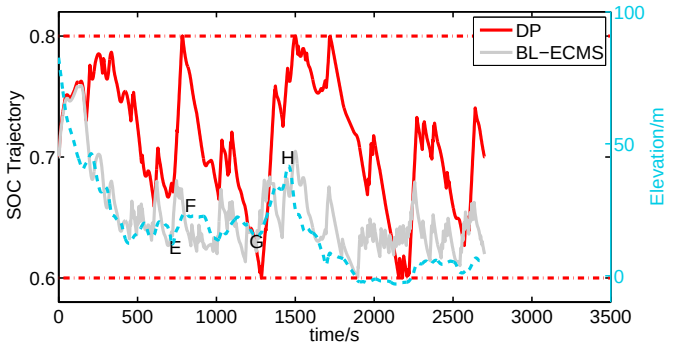

Figure 2.16: SOC trajectory with different control strategies (DP and BL ECMS) in the case with grade G6 and cruise speed 30mph. The solid and dashed lines show the SOC trajectory and road elevation respectively.

The use of future information not only helps save fuel, but may also reduce unnecessary charging and discharging of the battery. Reduced charge and discharge cycles may enhance the longevity of the battery. Figures 2.17 and 2.18 illustrate the percentage increase in the battery's charging and discharging power in the baseline ECMS and rule-based strategy respectively compared to the case with terrain preview.

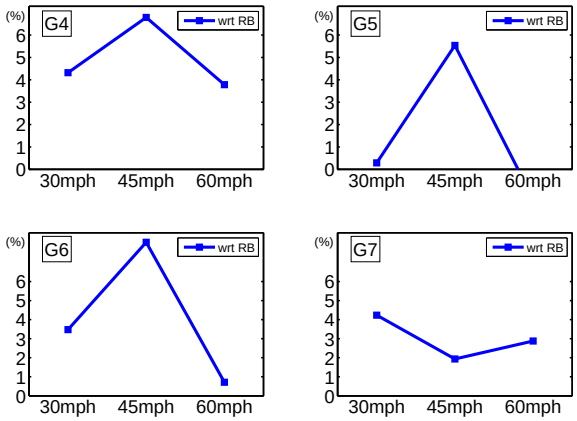

Figure 2.17: The percentage increase in the battery's charging and discharging power with baseline ECMS compared to DP with preview.

We observe that preview not only contributes to better fuel economy, but also reduces the battery's charge/discharge cycles. The amount of the reduction depends on the baseline control

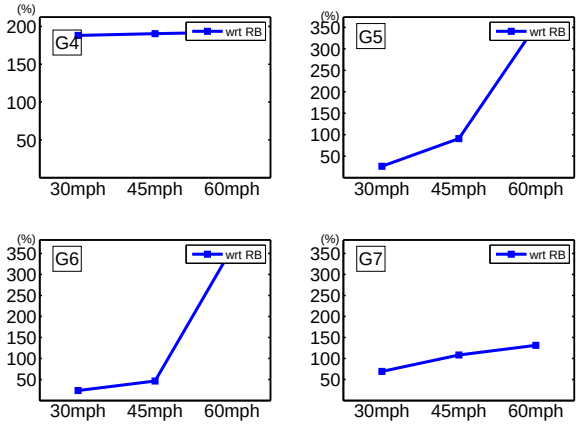

Figure 2.18: The percentage increase in the battery's charging and discharging power with rule-based without preview compared to DP with preview.

strategy: For baseline ECMS this is only 1-6% increase while with rule-based baseline this is 50-350% increase. In other words the baseline rule-based strategy seems to discharge and charge the battery aggressively to achieve good fuel economies; thus it can have negative influence on the battery's life. Quantifying the influence on the battery's life is an open question which is not in the scope of this discussion.

2.6 Conclusions

The role of terrain preview in reducing the fuel use of a parallel hybrid vehicle was investigated in this chapter. To focus the study on terrain preview only, the vehicle was assumed to cruise at a constant known velocity. Terrain preview and known velocity made possible calculation of *optimal* energy management decisions by solving a dynamic program or through an "optimal" ECMS strategy. The resulting fuel economy was then compared to that of two baseline strategies which lacked preview: a rule-based strategy representative of the approach common in industry and a modified ECMS strategy which is similar with the approach frequently used in academic papers. Some of the main conclusions are:

1. No big difference is seen between DP and ECMS with preview if the SOC trajectory does not exceed its bounds in the ECMS strategy.

2. For most simulation cases, the ECMS baseline achieves better result than rule-based control. Therefore the calculated impact of preview depends on the selected baseline strategy without

preview.

3. Simulations on hilly terrain shows an average fuel economy improvement of 1-4% is possible with terrain preview.

4. The improvement is inversely correlated to the cruise speed; i.e., it decreases at higher speeds.

5. The improvement depends on battery size. Simulation cases show improvement decreases for a larger battery pack.

6. Preview also reduces the average energy flow to and from the battery and therefore may increase the battery's life.

Chapter 3

Route Preview in Energy Management of Plug-in Hybrid Electric Vehicles

3.1 Introduction

Plug-in hybrid electric vehicles (PHEVs) are now making the transition from prototype concept to mass production. Plug-in versions of Toyota Prius for instance, are expected to go on sale in 2011-2012. Similar to conventional hybrid electric vehicles, PHEVs can take advantage of regenerative braking and a reduced sized engine operated more efficiently. In addition by partly utilizing the cheaper and typically cleaner electric grid energy, PHEVs achieve a much better overall fuel economy than conventional hybrid vehicles; their environmental footprint may also be much smaller. Added efficiency of a PHEV relies on its power management strategy, the algorithm which determines the split of the power request between the combustion engine and electric drive [66]. The focus of this discussion is on developing a real-time implementable power management strategy that uses terrain, traffic, and trip distance preview and can enhance energy utilization of PHEVs.

Typical power management schemes in production HEVs use rules, pre-optimized maps, or instantaneous optimization to reduce fuel use while sustaining the state of charge of the battery [74, 11, 22]. For this, they rely on instantaneous information about power demand and state of

the vehicle. This is formalized in a family of Equivalent Consumption Minimization Strategies (ECMS) first introduced by [53] where the power split ratio is found by an instantaneous optimization algorithm [37, 60, 65]. In a PHEV, unlike an HEV which maintains the battery's state of charge in a narrow operating band during the whole trip, maximum energy efficiency is achieved if the batteries are depleted to their minimum allowable charge by the end of a trip.

Existing energy management strategies for conventional HEVs cannot be directly transferred to a PHEV. It is possible to run the PHEV in its electric mode until the battery is nearly depleted and then switch to a charge sustaining mode and run the PHEV similar to an HEV [62, 10]. The result however may be far from optimal; it can be shown that the fuel optimal solution is one that blends use of the combustion engine and electric motor throughout the trip in a way that the battery is nearly depleted at the charging destination [62]. This in turn requires knowledge of future trip conditions such as trip length and future power demands. In [79] we found that knowledge of future road terrain profile is beneficial in energy management of HEVs. In [77] we showed that advance knowledge of trip length can contribute to fuel saving in PHEVs. Missing in our previous work [77] and [79] was a real-time implementable algorithm for systematic integration of long-horizon preview information.

With complete knowledge of future driving conditions, it is possible to generate the optimal energy management policy by solving a dynamic program (DP) such as in [43]. This however is computationally demanding and not suitable for the practical cases with only *partial* preview. The authors of [19] propose the use of a two-scale DP solution for a PHEV: A higher-level DP that plans the battery's state of charge (SOC) based on approximate information for the entire trip and a low-level shorter horizon DP that has more accurate information and tracks segmentally the SOC trajectory found at the higher level. While interesting, constraining the solution to track a "loosely" optimized SOC trajectory is a shortcoming of the approach in [19]; i.e. it does not fully adapt its policy to instantaneous values of the battery's SOC and driver demand.

Differently from previous work, this study first classifies four different levels of access to future information for power management of a PHEV: i) full knowledge of distance, future velocity, and upcoming terrain profile, ii) full knowledge of distance, upcoming terrain and estimated velocity, iii) knowledge of distance to the next charging station only, iv) no future information. Except for the first level with full future information, the paper proposes *real-time* control strategies. The real-time power management is decomposed to an instantaneous optimization and a (global) parameter

estimation: the power management decisions are calculated by a computationally efficient local ECMS optimization and based on instantaneous driver demand and the battery's state of charge. It is the unknown parameter of the local ECMS that depends on future driving conditions. With the second level of preview, local optimization parameters are estimated by a backward DP or backward ECMS sweep over the estimated future velocity and exact future 3D terrain information. With the third preview level, the parameter of local ECMS is adjusted based on remaining distance to the next charging station.

Section 3.2 presents the vehicle configuration and its simulation model. Section 3.3 summarizes the DP and ECMS control strategies and also includes description of a rule-based control strategy which is used as a comparison baseline. Section 3.4 proposes different *real-time* control algorithms in which ECMS is adopted for instantaneous optimization with parameters adjusted by different methods depending on the level of preview. In Section 3.5 two simulation case studies are presented which lead to conclusions in Section 3.6.

3.2 The PHEV Powertrain Configuration and Model

A midsize 2000kg passenger vehicle with a parallel hybrid electric configuration is selected for this study. Parameter values and detailed performance maps for various powertrain components were extracted from the database of Powertrain System Analysis Toolkit (PSAT) simulation software developed by Argonne National Laboratory [40]. A 120kW gasoline internal combustion engine and a 45kW AC motor were selected. They are directly connected to a torque coupler followed by a 5 speed automatic transmission. The auxiliary energy storage unit is a 21.5Ah lithium-ion battery pack, reasonably sized for a PHEV. The all-electric range for this configuration with 60% usable depth of discharge is about 20-30 km depending on the cycle. The key vehicle parameters are summarized in Table 3.1.

Table 3.1: Parameters of the simulated PHEV.

maximum engine power	120kW	maximum motor power	45kW
battery capacitance	21.5 Ah	open-circuit voltage	267 V
reducer ratio	2	final drive ratio	10.5

Recall the model of battery dynamics in energy management of an HEV:

$$\frac{d}{dt}SOC = -\frac{V_{oc} - \sqrt{V_{oc}^2 - 4P_{batt}R}}{2RC}, \tag{3.1}$$

This battery model as well as models for engine fuel consumption, motor input-output power, and gear shifting is kept the same as shown in Section 2.2 for an HEV.

3.3 Energy Management Strategy

A PHEV can be operated in two modes as shown in Figure 3.1: charge depleting (CD) and charge sustaining (CS). When the battery SOC is near its minimum value the PHEV is operated in the charge sustaining mode by blended operation of the engine and the electric motor. The battery state of charge is maintained near a set value similar to operation of a conventional HEV, therefore all the energy management strategies for HEV are transferable to PHEV in the CS mode.

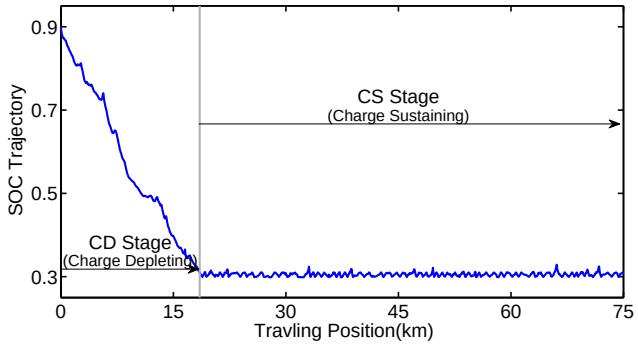

Figure 3.1: Schematic of PHEV operating modes.

When the battery SOC is high, the PHEV is operated in the charge depleting mode: the battery's charge is depleted to its minimum allowed value with either all-electric operation or blended operation of the electric motor and combustion engine [5]. Because the electric grid energy normally costs less than gasoline fuel energy, the ideal scenario is to run the PHEV in its all electric mode for short trips between two charging stations. For trips longer than the all electric-range blended operation of the electric motor and combustion engine throughout the trip is shown to be more fuel economical than all electric depleting followed by charge sustaining [62]. The decision to operate the PHEV in all-electric charge depleting mode or blended charge depleting mode can benefit from knowledge of future driving conditions.

3.3.1 Rule-based Control Strategy

When the future power demands are unknown, the vehicle is initially operated in all-electric charge depleting strategy. During this period the engine could be turned on if the power load exceeds the capability of the battery or the motor. When the battery nears minimum allowable charge, the operation is switched to charge sustaining mode for which we adopt a rule-based power management strategy from PSAT simulation software demonstrated in Section 2.4.1. Because of relative ease of tuning and implementation, rule-based power management strategies have been widely used in industry. Examples of different rule-based strategies can be found in research papers as well [43, 22, 57, 15, 45].

3.3.2 Optimal Control: DP and ECMS

Similar to conventional hybrid vehicles, maximizing the fuel economy of a PHEV can be explicitly formulated as minimization of the following cost function [22],

$$J_f = \int_{t_0}^{t_f} \dot{m}_f(t,u)dt + \phi(SOC_0, SOC_f) \tag{3.2}$$

subject to the powertrain model equations and the following constraints:

$$\begin{aligned} SOC_{min} \leq SOC \leq SOC_{max} \\ T_{eng}^{min}(\omega_{eng}) \leq T_{eng}(\omega_{eng}) \leq T_{eng}^{max}(\omega_{eng}) \\ T_m^{min}(\omega_m) \leq T_m(\omega_m) \leq T_m^{max}(\omega_m), \end{aligned} \tag{3.3}$$

where $\dot{m}_f$ is the fuel consumption rate; SOC_0 and SOC_f are the initial SOC and final SOC respectively; SOC_{min} and SOC_{max} are the minimum and maximum bounds on SOC; $T_{eng}^{min}(\omega_{eng})$ and $T_{eng}^{max}(\omega_{eng})$ are the minimum and maximum torque of the engine at given speed; $T_m^{min}(\omega_m)$ and $T_m^{max}(\omega_m)$ are the minimum and maximum torque of the electric motor at given speed; and $\phi(SOC_0,\ SOC_f)$ represents the amount of fuel equivalent to the difference between final and initial electric energy, stored in the battery. Analytical solutions to the above optimization problem do not exist in general, due to its many constraints and nonlinearities. We employ the two algorithms that are widely used for numerical solution of the optimal energy management problem.

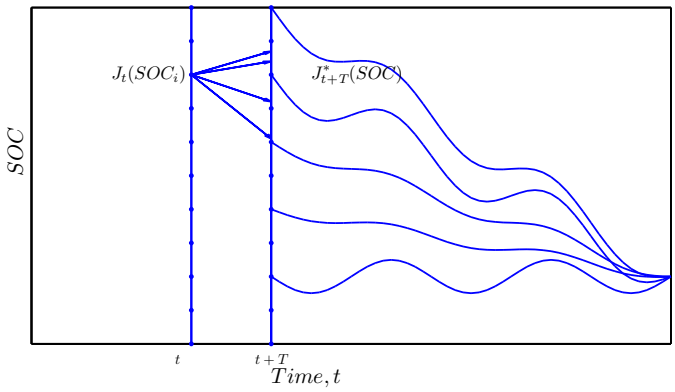

Figure 3.2: Illustration of DP algorithm

3.3.2.1 Dynamic Programming

In the ideal scenario that the future velocity and exact future power demand are known, the optimal power-split ratio that minimizes the cost function (3.2) subject to model equations and the constraints in (3.3) can be numerically obtained by solving a deterministic dynamic program [43]. The time horizon, the state variable SOC, and the power split ratio are discretized and the problem is solved backward in time according to the Bellman's optimality principle [7]. Figure 3.2 illustrates the methodology of DP algorithm in which:

$$J_t(SOC_i) = J^*_{t+T}(SOC) + L(u,t) \tag{3.4}$$

where T is the sampling time; $J_t(SOC_i)$ is the cost from initial SOC_i at time t to final desired SOC_f; $J^*_{t+T}(SOC)$ is the optimized cost from any initial state of charge at time $t+T$ to final desired SOC_f; and $L(u,t) = \dot{m}_f(t,u)$.
The control law u is obtained by:

$$u_{opt}(SOC_i, t) = arg\min\{J^*_{t+T}(SOC) + L(u,t)\} \tag{3.5}$$

This process is repeated for different pairs of (SOC_i, t) backward based on the calculation of minimized cost $J^*_{t+T}(SOC)$ at previous step $t+T$. For those points where the SOC does not exactly fall on the discretized SOC grid at time $t+T$, the minimum cost $J^*_{t+T}(SOC)$ is calculated from the interpolation of the neighboring grid points. The term $J^*_{t_0}(SOC_0)$ at time t_0 and initial state of charge SOC_0 is considered the global minimum of the cost in (3.2). For convenience of our

next discussion, the minimized cost pairs $J_t^*(SOC)$ in time domain are converted to $J_{X_t}^*(SOC)$ in spatial domain where X_t is the position at time t.

3.3.2.2 Equivalent Fuel Consumption Minimization Strategy

In the Equivalent Fuel Consumption Minimization Strategy (ECMS) the above optimization problem is simplified to minimization of the *instantaneous* (rather than integral) equivalent fuel rate $\dot{m}_{f,equ}$ defined as [57]:

$$\dot{m}_{f,equ} = \dot{m}_f + s \cdot P_e / H_f, \tag{3.6}$$

where P_e is the net power charged to the battery or the power drawn including the power loss to the electric circuit resistance; s is a fuel equivalent factor converting electric power to equivalent fuel power; and H_f is the lower heating value of the fuel.

With known future power demands, it is possible to find the true value for the equivalent factor s. This can be better understood by using Pontryagin's minimum principle. The Hamiltonian for the cost function (3.2) is:

$$H(SOC, \mathrm{u}, \mathrm{t}) = \dot{\mathrm{m}}_\mathrm{f} + \lambda(t) S\dot{O}C, \tag{3.7}$$

where $\lambda(t)$ is the co-state and its optimal value depends on future power demands. Following Pontryagin's minimum principle, the co-state λ has the following dynamics [69, 8]:

$$\dot{\lambda}(t) = -\frac{\partial H(SOC, \mathrm{u}, \mathrm{t})}{\partial SOC} = -\lambda(t) \frac{\partial S\dot{O}C}{\partial SOC} \tag{3.8}$$

subject to the equality constraint $SOC_f = SOC_d$. After substitution of the dynamics of the state of charge $S\dot{O}C = -\frac{I}{C}$ and $P_e = IV_{oc}$ in (3.7) we obtain,

$$H(SOC, \mathrm{u}, \mathrm{t}) = \dot{\mathrm{m}}_\mathrm{f} - \frac{\lambda H_f}{V_{oc} C} \frac{P_e}{H_f} \tag{3.9}$$

Defining:

$$s = -\frac{\lambda H_f}{V_{oc} C} \tag{3.10}$$

yields the same equation as in (3.6). The challenge in finding the correct value of s for any given cycle can be seen by observing its dependence on the co-state λ in (3.10). The optimal value of the co-state λ should ensure $SOC_f = SOC_d$ and this strongly depends on the upcoming power demands. Therefore the optimal value of s is a function of future driving conditions as well as the current value of the battery's state of charge. While, due to uncertain future power demands, the true value of s can not be found, we can come up with an estimate $\hat{s}$ by utilizing partial preview information, as described in the next section.

3.4 Estimation of Equivalent Factor With Partial Preview

This section describes how the equivalent factor s can be estimated by utilizing different levels of preview information. The estimate $\hat{s}$ replaces s in Eq. (3.6).

3.4.1 Optimal Control with Partial Preview: Future Terrain, Trip Length, and Estimated Trip Velocity

The future power demand is a function of upcoming road slope and future velocity profile. The road terrain information can be retrieved accurately from in-vehicle 3D maps and the vehicle GPS-based navigation system if the route is known a-priori. As for the velocity, it is possible to estimate it using real-time traffic data streams or by using historic traffic data [21, 20]. The focus in this part, however, is not on a method of velocity estimation; rather we focus on how such an estimate can be used online in energy management of PHEVs.

3.4.1.1 Estimating the Equivalent Factor Using DP

From Hamilton-Jacobi-Bellman equation, we know that the partial derivative of the optimal cost with respect to the state is equal to the co-state λ [69, 8], that is:

$$\lambda(SOC, x_t) = \frac{\partial J^*_{x_t}(SOC)}{\partial SOC} \tag{3.11}$$

Therefore, using Eq. (3.10), (3.11) we have,

$$s(SOC, x_t) = -\frac{\partial J^*_{x_t}(SOC)}{\partial SOC}\frac{H_f}{CV_{oc}} \tag{3.12}$$

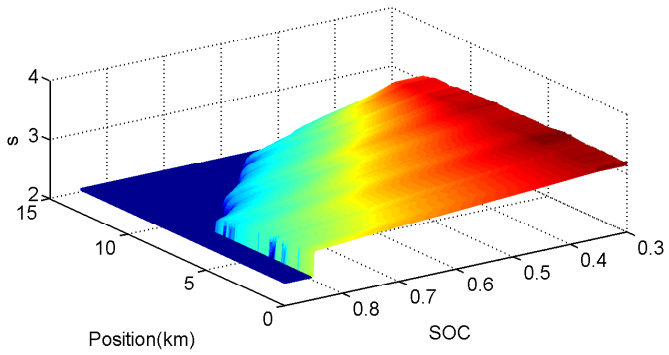

Figure 3.3: Equivalent factor s as a function of SOC and position in the 3D plane.

With an estimate of future power demand, it is possible to execute a dynamic program backward in time which will calculate, for any possible pair (SOC, x_t), an estimate of the optimal cost-to-go denoted by $\hat{J}^*_{x_t}(SOC)$. Finally, the estimate $\hat{s}$ is expressed as:

$$\hat{s}(SOC, x_t) = -\frac{\partial \hat{J}^*_{x_t}(SOC)}{\partial SOC} \frac{H_f}{CV_{oc}} \tag{3.13}$$

Because DP calculates the cost-to-go backwards in time, the $\hat{s}$ value obtained from the above formula will not depend on the past but only on future power demands. Thus a single round of DP computations may be enough for a trip as long as the estimated future power demand does not change significantly. Figure 3.3 maps out values of $\hat{s}(SOC, x_t)$ calculated using Eq. (3.13) for a simulation case which is used later in our discussion. In the figure, a low $\hat{s}$ value implies using electric power is cheaper than using fuel and therefore encourages use of the battery. A high $\hat{s}$ value on the other hand discourages use of battery. As it can be seen in Fig. 3.3, the value of $\hat{s}$ is mostly between 2 and 3.2 but drops at high SOC values or when the trip is nearly complete. In other words the controller discharges the battery more aggressively, when it anticipates that the charge left in the battery meets the energy needed to reach the destination. The value of $\hat{s}$ depicted in 2D at different positions is shown in Fig.3.4. It can be seen that the s-curve becomes steeper and more sensitive to the battery SOC when the vehicle approaches its destination. We refer to this method of estimating the equivalent factor by using DP as D-ECMS in the next discussions.

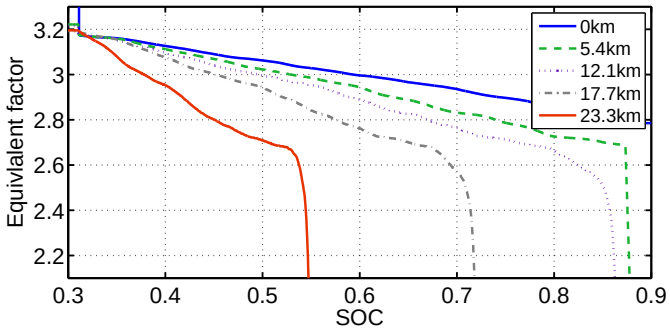

Figure 3.4: Equivalent factor s as a function of SOC at different positions in a 2D plane.

3.4.1.2 Estimating the Equivalent Factor Using Backward ECMS

Online calculation of the equivalent factor using dynamic programming is viable but requires at least one backward sweep which depending on the selected grid size and the processor can be computationally demanding. In order to cut the computational load, here we propose use of a backward ECMS, inspired by DP, for estimating the s value. It is possible to run the ECMS backward in time starting from the final desired state of charge SOC_d and iterate on the value of s that yields the present state of charge. More specifically we propose the following steps:

1. The equivalent factor s range $[s_e, s_0]$ is estimated as in [77], where s_e is the conversion ratio of fuel and electricity price explained in section 3.4.2; s_0 is the neutral equivalent factor for a charge-sustaining HEV [79].

2. The range $[s_e, s_0]$ is discretized and the optimal SOC trajectory is obtained backward for each discretized s value in this range starting with the final state of charge $SOC_f = SOC_d$. By change of time variable $\tau = t_f - t$ the SOC dynamics in (3.1) and co-state dynamics in (3.8) can be rewritten backwards-in-time:

$$\frac{d}{d\tau}SOC = \frac{V_{oc} - \sqrt{V_{oc}^2 - 4P_{batt}R}}{2RC} \tag{3.14}$$

$$\frac{d}{d\tau}\lambda = -\lambda(\tau)\frac{\partial(\frac{dSOC}{d\tau})}{\partial SOC} \tag{3.15}$$

However, this is a two-point boundary value problem and computationally expensive due to the coupling of the SOC and co-state dynamics in (3.1) and (3.15). To reduce the computation

time for online implementation, the co-state and as a result the equivalent factor may be assumed to be constants in each backward run of ECMS. This is a valid assumption if, i) the pointwise-in-time constraints on SOC are relaxed, and ii) the right-hand side of SOC dynamics in Eq. (3.1) is not an explicit function of SOC. The latter is true when the open circuit voltage of the battery V_{oc}, and the battery resistance R, and capacitance C, are constants. These assumptions yield $\dot{\lambda}(\tau) = 0$ and a constant optimal equivalent factor s. Because of large variation of SOC in a PHEV, assumption of a constant V_{oc} may not be valid. We show in the Appendix that when variation of V_{oc} is considered, the optimal value of λ varies considerately over an entire trip, but not the equivalent factor s. The variation of optimal s is much less than that of λ, therefore s could be approximated as a constant through the trip. Also, we note that the estimation error of the future driving conditions may have a larger impact on the equivalent factor than variation in battery parameters and therefore the latter may not very much influence the results. At each position x_t and based on the latest preview information the backward ECMS is executed starting with the final state of charge of SOC_d; this is repeated for different choices of $s \in [s_e, s_0]$. Each run results in an optimal SOC trajectory which is a function of choice of s_i and position x_t as shown in Fig. 3.5.

3. The value of s that yields the present SOC of the battery is selected as the optimal value. Interpolations are performed when necessary. Note that this optimal value will be recalculated at each step in time based on the latest preview information.

The computation time for the above backward ECMS approach on a personal computer is much smaller than running the DP and thus it is thought to be very promising for real-time implementation. Besides, because of its faster execution, the prediction of the future can be updated periodically which potentially enhances the performance of this methodology. We refer to this method of estimating the equivalent factor by a backward ECMS as E-ECMS.

3.4.2 Optimal Control with Partial Preview: Distance to Next Charging Station

A desired scenario is to estimate the equivalent factor without using 3D terrain and velocity information. In [54, 79, 64] different methods were proposed for estimating equivalent factor in a charge sustaining HEV. Because in the PHEV case, the batteries can also be charged from the

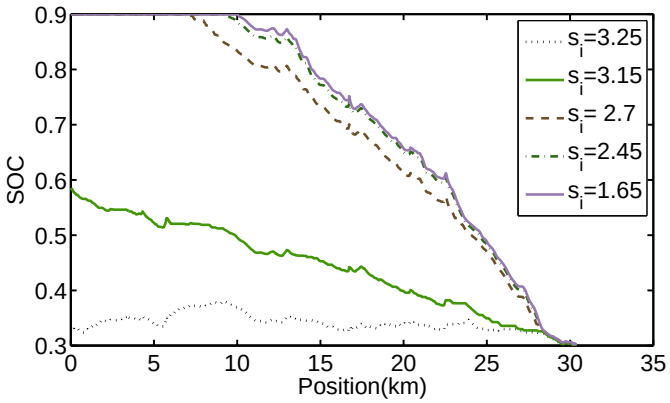

Figure 3.5: Optimized SOC trajectories with the same terminal SOC_f and different initial guesses for equivalent factor s_i.

electric power grid, the above approach for estimating the equivalent factor s does not directly apply. A fair evaluation of s can benefit greatly from i) information about the distance to the next charing station as compared to the all-electric range of the vehicle and ii) price of grid energy as compared to price of fuel energy. Remember s, by definition, is the conversion ratio between the electric power and fuel. Therefore the first step is to find the price ratio r between electric power and fuel defined by:

$$r = \frac{Pr_f s_0 C_s/(\rho H_f)}{Pr_e/\bar{\eta}_e}, \tag{3.16}$$

where Pr_f is the fuel price ($\$/l$); ρ is the density of the fuel (kg/l); H_f is the lower heating value of fuel (J/kg); $C_s = 3.6 \times 10^6$ is the constant conversion ratio between kWh and $Joules$; Pr_e is the electricity price ($\$/kWh$); $\bar{\eta}_e$ is the charging efficiency from charging station to PHEV. s_0 is the estimated conversion ratio from fuel to electricity for a charge sustaining HEV [79] based on the average efficiency of the powertrain.

When the traveling distance is known to be less or equal to the vehicle's electric range, the powertrain can be run in its all electric mode. The equivalent factor s_e for this mode is then calculated as:

$$s_e = \frac{s_0}{r} \tag{3.17}$$

Combining Eq. (3.16) and (3.17) yields:

$$s_e = \frac{Pr_e/\bar{\eta}_e}{Pr_f C_s/(\rho H_f)} \tag{3.18}$$

Note that in above equation, s_e is not a function of the neutral equivalent factor s_0. On the other hand when the traveling distance is known to exceed the electric range, the equivalent factor should be adjusted up to reflect use of gasoline fuel energy during the trip. Based on the nominal all-electric range X_e and the total trip distance X we define:

$$\kappa = \min(\frac{X_e}{X}, 1) \tag{3.19}$$

and determine an average adjusted equivalent factor s_{adj} as an initial guess:

$$s_{adj} = s_e + \sqrt{1-\kappa^2}(s_0 - s_e) \tag{3.20}$$

In the above equation when $X_e \geq X$ then $s_{adj} = s_e$ reflecting the fact that all the electricity will be provided by the grid. In the other extreme, when the electric range X_e is much smaller than the distance to the next charging station X so $\kappa \approx 0$, then $s_{adj} = s_0$ which reflects the average electric price in the charge sustaining mode. In between, when $0 < \kappa < 1$, a value between s_0 and s_e is chosen as the base equivalent factor.

To reflect the influence of current SOC in selection of equivalent factor, one can redefine the parameters κ and s_{adj} as follows:

$$\kappa(t) = \min(\frac{x_e(t)}{x_r(t)}, 1) \tag{3.21}$$

$$s_{adj}(t) = s_e + \sqrt{1-\kappa(t)^2}(s_0 - s_e), \tag{3.22}$$

where $x_e(t)$ is the all-electric range for the remaining SOC and $x_r(t)$ is the remaining trip distance. They are defined as:

$$\begin{aligned} x_e(t) &= \frac{SOC - SOC_{min}}{SOC_{max} - SOC_{min}} X_e \\ x_r(t) &= X - x_t \end{aligned} \tag{3.23}$$

By definition, the equivalent factor varies between s_e and s_0 depending on the current SOC and remaining trip distance. The dependence of the s value on four parameters s_0, s_e, SOC, and remaining trip distance $x_r(t)$ reduces its sensitivity to the accurate estimation of s_0; this is unlike a charge sustaining HEV. The ECMS discussed in this part is referred as B-ECMS since it blends operation of the engine and electric motor and discharges the battery gradually. This is similar to the methods proposed in [71, 77] but without the assumption of tracking a pre-defined SOC trajectory.

3.4.3 Optimal Control Without Preview

In absence of preview, one can guess a low value for the equivalent factor initially and increase it when SOC decreases. This ensures that the electric power is discharged more aggressively at high SOC and conservatively at low SOC. When the SOC reaches its lower bound, the control strategy is switched to a charge sustaining strategy. In the next discussion, we refer to this strategy as DS-ECMS (depleting and sustaining ECMS). This is shown in Figure 3.6 where the equivalent factor s is chosen to be a linear function of SOC in charge depleting (CD) stage and a piece-wise linear function in charge sustaining (CS) stage with details shown in [79]. A summary of different control strategies as well as their abbreviations is shown in Table 3.4.

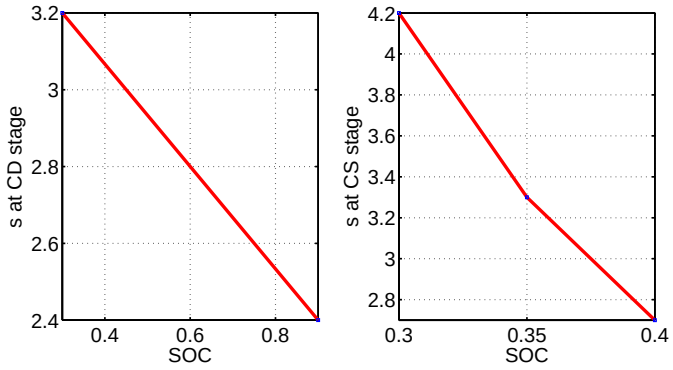

Figure 3.6: Equivalent factor s as function of s at different stages: charge depleting (CD) stage and charge sustaining (CS) stage.

3.5 Simulation Analysis

The performance of the proposed methods is studied via two sets of simulations, one with a federal test cycle and a real-world terrain profile and one with velocity and terrain data obtained

simultaneously when driving in a mountainous area. The total energy cost, taking into account both fuel and electricity cost, is used as the index for evaluating the performance of different strategies . The price of gasoline and electricity power, which may vary by area and time, are set to 0.79\$/$litre$ (3\$/$gallon$) and 0.12\$/kWh respectively.

3.5.1 Case Study I

The terrain and velocity profile for this simulation case study are shown in Fig. 3.7. The terrain is a stretch of uphill road in Contra Costa County in California and is extracted from Intermap Technologies' 3D map database and the velocity profile is that of EPA Highway Fuel Economy Cycle (HWFET). Because the fuel economy of a PHEV strongly depends on the trip distance, three simulation distances of 32km, 48km, and 72km are selected which are respectively 1.6, 2.4, and 3.6 times the all-electric range. The velocity profiles are repeated for long distance simulations; the grades are mirrored, and then also repeated if necessary. A simple method to estimate the velocity is deployed in which the vehicle is forced to run with the speed limits along the road. In the simulation the speed limits, observed from HWFET cycle, are selected at $20m/s$ and $25m/s$ for the two different segments. The acceleration/deceleration of the vehicle is set to the constant value $0.5m/s^2$. The real and estimated velocity profiles are shown in Fig. 3.7. In practice it is deemed feasible to estimate a vehicle's future speed by using known speed limits, traffic signal location and timing information, and real-time traffic flow conditions [19].

In each simulation case study, dynamic programming with full future information can find the lowest energy cost; we use this lowest cost as the best benchmark. The performance of other proposed methods is evaluated by calculating their percent energy cost difference with respect to the DP benchmark. Table 3.2 summarizes these results. When preview is available the cost gap of different control strategies compared with DP is mostly around or less than 1%. It also interests us to determine which level of future information is more important for reducing the energy cost. It can be seen that B-ECMS with only trip distance information performs very close to D-ECMS and E-ECMS and is not far from the best possible benchmark, implying that knowledge of trip distance is a significant factor for energy cost saving for a PHEV. Without preview, the energy cost would increase considerably as shown in the results of DS-ECMS and rule-based strategies.

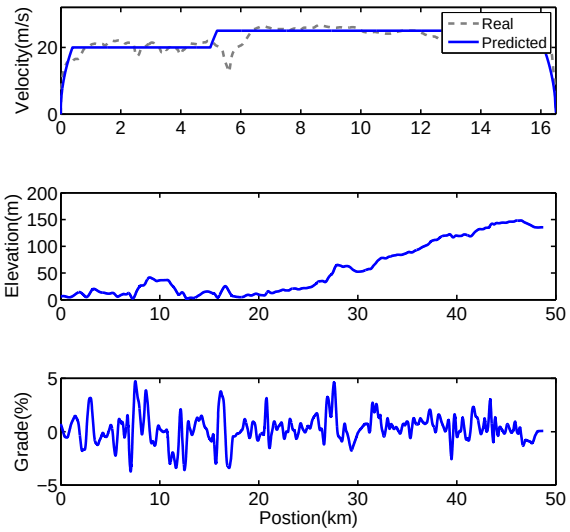

Figure 3.7: Velocity, elevation, and grade profiles for Case Study I

Table 3.2: Performance gap (%) of different control strategies compared with DP with trip distance of 32km, 48km, 72km for case study I.

Gap(%)		32km	48km	72km
preview	D-ECMS	0.73	0.66	0.39
	E-ECMS	0.76	0.69	1.18
	B-ECMS	1.62	0.65	0.91
no preview	DS-ECMS	2.90	2.67	3.59
	Rule-based	8.88	7.88	8.61

3.5.2 Case Study II

To evaluate the influence of larger changes in elevation, we drove a vehicle starting from the city of Clemson in South Carolina to the town of Highlands in North Carolina and back, mostly via the hilly US-28 road on May 14th, 2010. The elevation change in this trip was more than 900 m over a distance of almost 50 km. We recorded both the velocity and elevation using a Garmin GPS 20x receiver with a sampling time of 1 second. The raw data from the GPS were refined by removing the dead points and by interpolating the missed data. For the simulation case study, we divide the trip into three different segments all having the same trip length (48km) with a combination of uphill and downhill profiles (*Route 1*), an uphill profile (*Route 2*), and a downhill profile (*Route 3*) as shown in Fig. 3.8. The predicted speed in this figure reflects the speed limits observed from the road side signs which we had recorded separately as a function of trip time. To isolate the influence of velocity, we also designated a fourth scenario denoted by *Route 4* with the same velocity profile

of *Route 2* but with road grade set to zero.

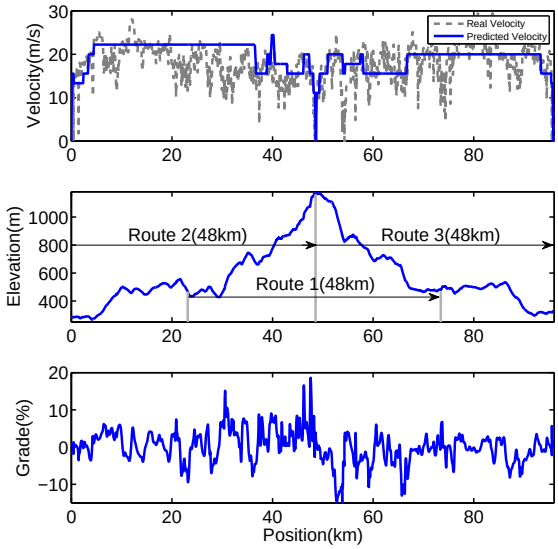

Figure 3.8: Velocity, elevation, and grade profiles for Case Study II.

Similar to case study I, DP with full future information is used as the best benchmark. Table 3.3 summarizes the energy cost gap between strategies with and without preview and the DP benchmark. Here D-ECMS results are not reported as they are similar to those of E-ECMS. As shown in the table, E-ECMS performs closest to DP for the R2 uphill terrain with the performance gap of only 1%. The difference is larger for the R3 downhill terrain (6.46%) and for flat case of R4 (6.33%). Note that on steep uphill roads the power demand from the grade dominates that of demand to changes in velocity; thus poor estimation of velocity may have less influence on the optimality of E-ECMS solution. On downhill or flat terrain on the other hand the power demand caused by changes in velocity dominates and therefore the uncertainty about the future velocity profile results in larger performance gaps between E-ECMS and DP.

As seen in this table, the trip distance based B-ECMS strategy is far from optimal especially when there are large downhill elevation changes (e.g. 40% worse than DP for R3). During downhill descents there is frequent opportunities for running electric only or for regeneration; but because B-ECMS estimates the fuel equivalent factor based on remaining trip distance only, it fails to capture part of the available potential energy. Observing this fact, here we propose an adjustment to the B-ECMS strategy to account for the influence of large elevation changes. Note that the free potential energy in downhill descents is equivalent to charging the battery from the power grid; therefore we

propose to adjust the B-ECMS strategy by correcting the all-electric range $x_e(t)$ as follows:

$$x'_e(t) = x_e(t) + \frac{mg\Delta h\bar{\eta}_r/(\bar{V}_{oc}C)}{SOC_{max} - SOC_{min}}X_e, \tag{3.24}$$

where m is the mass of the vehicle; $\bar{V}_{oc}$ is the average battery voltage; $\bar{\eta}_r$ is the average recuperation efficiency; we set $\bar{\eta}_r = 1$ when no recuperation is anticipated in the downhill descent. Δh is the the downhill elevation change and defined as: $\Delta h = \max\left(H(\tau > t)\right) - H(t_f)$, where $H(\bullet)$ is the elevation at time $(\bullet)$, t denotes the current time, and τ is the future trip time. In this equation, the net potential energy gain between top of a hill and end of the trip is converted to an equivalent all-electric range extension.

The performance of adjusted B-ECMS for routes R1 and R3 is shown in Table 3.3 and is much improved. Note that E-ECMS sometimes performs worse than (adjusted) B-ECMS. This may be attributed to large velocity transients in this case study which cannot be merely captured by using the speed limit approximation as done in E-ECMS. We observe that the algorithms with partial preview always perform better that strategies without preview.

Table 3.3: Performance gap (%) of different control strategies compared with DP in Case Study II(R1-Route 1, R2-Route 2, R3-Route 3 in Fig. 3.8, R4-flat road with velocity from R2)

Gap(%)		R1 uphill & downhill	R2 uphill	R3 downhill	R4 flat
preview	E-ECMS	2.74	1.03	6.46	6.33
	B-ECMS	8.53	2.81	39.56	2.77
	B-ECMS (adjusted)	0.75	-	5.00	-
no preview	DS-ECMS	7.28	4.82	16.55	8.34
	Rule-based	14.20	14.81	20.77	15.70

The performance of B-ECMS depends on the parameters estimation of s_0 and s_e. Generalization of this method to any other PHEV with real driving cycle needs further investigation. In D-ECMS and E-ECMS, no parameter tuning is necessary but estimation of the trip velocity is required.

3.5.3 Computational Case Study

Besides the energy cost, we also compared the computational burden in a simulation with total trip time of 1472 seconds and sampling time of 2 seconds. The SOC resolution was chosen at 0.0001 in all simulations. The simulations were performed on a personal computer with the

CPU speed of 1.8 GHz and memory of 2GB. Table 3.4 summarizes the computational time of each algorithm. It can be seen that the E-ECMS approach runs much faster than D-ECMS with the same level of preview without much loss in performance and has the potential to be used in real-time. The computational burden of B-ECMS and DS-ECMS is essentially the same as a normal ECMS approach and thus it is suitable for online optimization.

Table 3.4: Computational case study for proposed control strategies

Algorithm	Method to estimate equivalent factor s	CPU time (seconds)
D-ECMS	by DP	600
E-ECMS	by ECMS	2.5
B-ECMS	by blending operation	0.7
DS-ECMS	by depleting and sustaining operation	0.7

3.6 Conclusions

This part work investigated real-time implementable energy management algorithms for energy management of plug-in hybrid vehicles that can take advantage of information preview for fuel saving. This is achieved by handling the energy minimization problem at two levels: i) A global optimization approach that utilizes preview information (if available) for the whole trip to estimate a fuel-electricity equivalent parameter, and ii) a local ECMS optimization which determines the optimal control based on instantaneous values of power demand, battery state of charge, and the parameter set by the global optimizer. A simulation case study with a federal driving cycle-HWFET indicated that knowledge of distance to the next charging station can have a significant influence on the fuel economy of a PHEV because it allows better planning of all-electric or blended motor/engine operation. Full terrain and estimated future velocity can result in additional fuel economy improvement up to 1%. Another simulation case study with large elevation changes indicated the importance of accounting for potential energy gains resulting from significant elevation change. Predicting the future velocity profile based on speed limits helps the energy management of a PHEV in general. But if the real driving cycle has more velocity transients than the predicted one, the control strategy that relies only on trip length and elevation change and not on velocity estimate may perform better. The computational time required to include preview are shown to be much smaller than the total simulation time and therefore has the potential for real-time implementation. This work only focused on energy minimization. Future work can consider other factors such as total emissions by the vehicle and the electric grid.

Chapter 4

Traffic Flow Information Preview for Fuel Saving and Emission Reduction

4.1 Introduction

Today's advances in telematic and traffic information technology can be used to enable safer, smarter, and greener driving patterns [58, 12]. Vehicles capable of communicating wirelessly to the infrastructure and neighboring vehicles will be able to manoeuver more predictively, enhancing their safety and fuel efficiency. Some examples of this are the use of cooperative vehicle wireless communication for lane change, platooning, and obstacle avoidance [41, 34]. In [78, 80] it is shown how advanced telematics can be an enabler for better energy management of hybrid and plug-in hybrid vehicles.

Moreover, information can be transmitted wirelessly from individual vehicles to estimate the state of macroscopic traffic flow [75] and perhaps even enable higher resolution microscopic prediction about neighboring vehicles. In a microscopic traffic level, a vehicle of interest, say car n+1, is assumed to follow the car ahead, say car n as shown in Fig. 4.1. The key problem for optimal control purpose is to predict the velocity profile of car n over a short future horizon. Such prediction can in turn be used by individual vehicles, running in adaptive cruise control mode,

to reduce their velocity transients and undesirable stops and starts [38] leading to improved fuel economy, emissions, and ride comfort. Other recent work has proposed using information about upcoming terrain [25, 29] and information about the state of traffic signals [4, 49] to enhance the following vehicle's fuel economy in the adaptive cruise control mode.

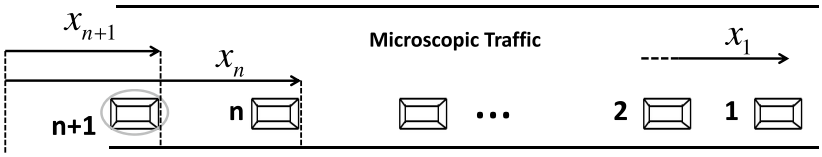

Figure 4.1: Microscopic car following traffic model

Not only the immediate driving condition of the lead car influences the driving behavior, but also the traffic pattern en route. Many of such stop and go conditions occur due to lack of information about the upcoming traffic pattern down the road. Many drivers choose to aggressively speed up to near the speed limit, only to be forced to abruptly decelerate their vehicles when faced with the slower traffic ahead of them and then perhaps idle or crawl in slow-moving traffic. If the upcoming traffic pattern is somehow "revealed" to the drivers in advance, the opportunity exits to adjust the speed more predictively to reduce harsh deceleration and idling or crawling intervals. Such planning of velocity could lower fuel use and emissions, improve the ride, and reduce brake and engine wear.

Such traffic pattern may be affected by traffic light timing, traffic jam occurrence, traffic wave evolution, local traffic events, weather condition, or even the road geometry. In the context of networked and "informed" vehicles, it is desired to predict all these factors or at least some of them. However, use of these different kinds of information is not apparent and needs to be organized. This can be done by classifying the prediction into different levels according to its time-scale and importance to the driver. Similar to transportation research area where traffic models are classified into three levels: microscopic level, mesoscopic level, and macroscopic level according to the level of details representing the traffic systems [27], we also classify the prediction of future driving conditions into three levels, i.e. microscopic level, mesoscopic levels, and macroscopic levels as shown in Fig. 4.2.

The microscopic level prediction refers to the prediction of the driving conditions surrounding a vehicle including the information of speed limits, stop sign, upstream traffic, and preceding car condition with a prediction horizon around 10-30 seconds. The microscopic traffic has relatively

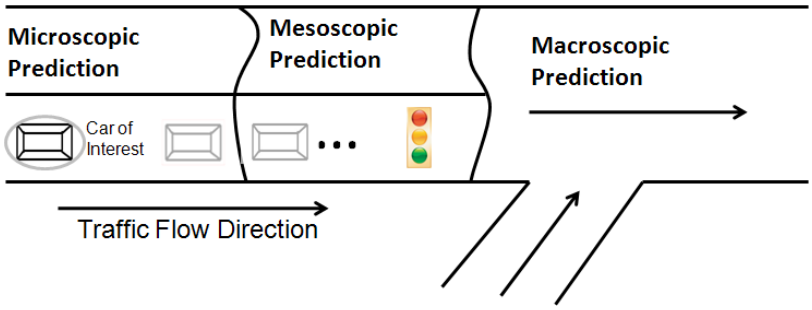

Figure 4.2: Schematic of microscopic, mesoscopic, and macroscopic traffic

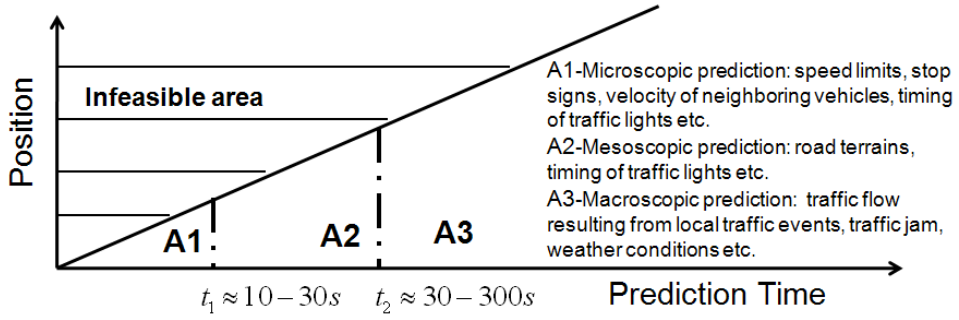

Figure 4.3: Multiscale spatiotemporal traffic prediction

fast dynamics and impose significant constraints on each driver. For example, sudden braking of preceding car will push the upstream vehicle to slow down. Thus this level is the most important prediction part in autonomous driving. Mesoscopic level refers to the driving conditions in near future with a horizon around 30-300 seconds, which is less important than the microscopic level, but may have significant influence for fuel saving. Examples of utilizing this level of prediction have been shown in [4,49] for utilizing traffic light prediction and in [29,25] for terrain prediction in heavy vehicles; the fuel consumption was reduced up to 10% and 3% respectively. Macroscopic level traffic models describe the average behavior of the traffic e.g. traffic density, traffic flow, and traffic speed. Different approaches e.g. model-based and data-based could be used to predict the traffic condition at a macroscopic level. The former predicts the traffic by gas-kinetic models, which will be discussed in Section 4.3; the latter predicts using historic and real-time traffic data. Figure 4.3 shows the traffic prediction in different scales.

Different levels of predictive information could be used in different ways. For example, microscopic traffic predictions could be integrated in the Adaptive Cruise Control Systems (ACC) for reducing stop and goes. The optimal vehicle velocity with mesoscopic and macroscopic information

prediction could be suggested to the driver via the add-on accessories such as the smart phone or intelligent speed assistant systems or simply used as a high-level reference speed to the adaptive cruise control system.

In next two sections, we will introduce a two level velocity planning algorithm based on microscopic and macroscopic traffic predictions: A predictive cruise control algorithm with a stochastic microscopic prediction and a velocity planning controller based on the preview of macroscopic information.

4.2 Predictive Cruise Control with Probabilistic Constraints for Eco Driving

The adaptive cruise control (ACC) systems in production cars today are intended to reduce the driver's workload and improve vehicle safety. Unlike a conventional cruise control system, an ACC system uses radar to measure the distance to a leading vehicle and can adjust the desired velocity to maintain a safe distance. While most ACC designs are based on instantaneous measurement of the inter-vehicular gap, it has been shown that predictive control strategies can result in smoother following velocity [28, 42, 81]. In such a predictive adaptive cruise control system, a major challenge is estimating the future driving pattern of the lead car.

To deal with the lead vehicle velocity uncertainty problem, in our work we employ a chance constrained model predictive control framework for the ACC in which the inter-vehicle distance constraints are imposed probabilistically. The velocity of the lead car is predicted stochastically using a Markov chain assumption; i.e. it is assumed that the velocity at the next sampling time only depends on the current step velocity and is independent of the past. The probability distribution of the velocity of the lead car over the prediction horizon is then found via Monte Carlo simulations. The lead vehicle is assumed to wirelessly share this information with neighboring vehicles. Knowledge of the velocity distribution of the lead car allows for the chance constrained MPC problem to be converted to a deterministic linear MPC problem for which efficient real-time solution methods exist.

The sections of this part are organized as follows: Section 4.2.1 introduces the car following model and vehicle longitudinal dynamics. In Section 4.2.2, the model predictive cruise control problem with stochastic constraints is presented. Simulation case studies are given in Section 4.2.3 and the the summary of the findings are in Section 4.4.

4.2.1 The Vehicle Model

4.2.1.1 Car Following Model

A variety of methods exist in the literature which model a car that follows a leading car, e.g. safe-distance models, stimulus-response models, and psycho-spacing models [27]. In this work we assume a safe-distance following model in which the follower maintains a velocity dependent gap

with the lead car:

$$D(t) = r(t) - x(t) \geq L_{min} + Tv, \tag{4.1}$$

here $r(t)$ and $x(t)$ are the position of front and following cars respectively; L_{min} is the minimum distance and usually is estimated as $L_{min} = \frac{1000}{\rho_{jam}}$, where ρ_{jam} (*vehicles/km*) is the density of traffic jam; T is the reaction time constant; and $v = \dot{x}$.

4.2.1.2 Vehicle Kinematics

The vehicle longitudinal motion is modeled based on simple kinematic relationships and a first order lag between acceleration command and actual acceleration:

$$\begin{cases} \dot{x} = v \\ \dot{v} = a \\ \dot{a} = -\frac{1}{\tau}a + \frac{1}{\tau}u(t) \end{cases}, \tag{4.2}$$

where $u(t)$ is the control input and can be understood as the steady-state acceleration command and τ is a time constant. The state vector is denoted by $z = [x \quad v \quad a]^T$. The discretized state-space model can be written as :

$$z(k+1) = A_d z(k) + B_d u(k), \tag{4.3}$$

where A_d and B_d are the discretized system matrices.

4.2.2 Control Problem Formulation

A model predictive control approach is used for the cruise control of the follower vehicle. To clarify the notations between the real states and predicted states, we use $z(i+k|k)$ denoting the i step prediction of z from time step k. The state dynamics of the following car is predicted by Eq. (4.3) as function of control input u as:

$$z(i+k|k) = \bar{A}(i)z(k) + \bar{B}(i)U, \tag{4.4}$$

where $U = [u(0+k|k) \quad ... \quad u(i+k|k) \quad ... \quad u(N_c-1+k|k)]^T$ and N_c is the number of steps of control horizon; beyond which the control inputs are assumed to be zero. Matrices $\bar{A}(i) \in R^{3\times 3}$, $\bar{B}(i) \in R^{3\times N_c}$ are obtained as functions of A_d, B_d.

At each time step k, a cost J, which may be a function of predicted states, control inputs, and the reference input is optimized yielding the optimal control input $u^*(i+k|k), i = 0 \quad ... \quad N_c-1$. But only the first control input of this sequence, $u^*(i+k|k), i = 0$, is applied and the calculations are repeated with the new initial conditions. Of course, the optimization should also satisfy the constraints imposed by systems design requirements.

Note that in our problem, the cost function and the constraints may be the function of the preceding car position $r(t)$, which is uncertain. With assumption of exact knowledge of $r(t)$, we can solve it as a standard MPC problem. In practice, however, $r(t)$ is not exactly known in advance and needs to be predicted. This could be done either in a deterministic way or stochastic way. In this study, we propose to predict $r(t)$ stochastically yielding a stochastic MPC problem. In order to evaluate the proposed methodology, a passive car following model is also developed for comparison.

4.2.2.1 Cost Function

The goal is to reduce fuel consumption without sacrificing drivability and following behavior. Instead of minimizing the fuel consumption directly, which is a highly nonlinear problem, we will minimize the acceleration over the prediction horizon. The effectiveness of this cost function is tested separately through the use of a commercial vehicle powertrain simulation software-Powertrain Simulation and Analysis Toolkits(PSAT)-developed by Argonne National Laboratory [40]. Moreover, we penalize the car following error at the end of each prediction horizon N_p. This can be achieved by the following cost function:

$$\begin{aligned} J = & \sum_{i=0}^{N_c-1} u^2(i+k|k) \\ & + q\{r(N_p+k|k) - x(N_p+k|k) - T\dot{x}(N_p+k|k) - L_{\min}\}, \end{aligned} \tag{4.5}$$

where q is the penalty weight for car following distance error. Other forms of cost functions can be found in [42, 28]. Note that we have a quadratic cost for acceleration but only a linear cost for tracking error. The gap constraints introduced later will ensure that this linear term remains positive.

By substituting the Eq.(4.4) into Eq.(4.5) and defining $\Gamma = [1 \quad T \quad 0]$, the cost function can be written as:

$$\begin{aligned} J = & \sum_{i=0}^{N_c-1} u^2(i+k|k) \\ & + q\{r(N_p+k|k) - \Gamma z(N_p+k|k) - L_{\min}\} \\ & = \mathrm{U}^{\mathrm{T}} \Lambda U - q\bar{B}(N_p)U + C, \end{aligned} \tag{4.6}$$

where $C = q\{r(N_p+k|k) - \Gamma \bar{A}(N_p)z(k) - L_{\min}\}$.

As we can see, the term C is independent of the control input u. Using a linear cost for following distance in Eq. (4.5) keeps the control input decoupled from the future position of front car. As a result, the position of the leading car, which is not a function of control input can be dropped from the cost function. If the following distance error cost has a quadratic form as in [6], the cost function will be coupled with the position of the lead car, complicating the next steps of this derivation.

4.2.2.2 Constraints

With the cost function in a quadratic form in Eq. (4.6), we now need to consider the constraints imposed by vehicle system limitations and safety requirements: the maximum and minimum acceleration constraints, non-negative velocity, maximum velocity constraints, and safe following distance. Specifically, the constraints on control input are formulated as:

$$u_{\min} \leq u(i+k|k) \leq u_{\max}, \tag{4.7}$$

for $i = 0, 1, 2...N_c - 1$, where u_{min} and u_{max} are the minimum and maximum allowable acceleration respectively.

The constraints for velocity are expressed as:

$$v_{min} \leq v(i+k|k) \leq v_{max}, \tag{4.8}$$

for $i = 1, 2, ...N_p$, where v_{min} and v_{max} are minimum and maximum velocity, and v_{min} is set to 0 in our study.

With the position of the front car, $r(t)$, exactly known or with deterministic prediction, the car following distance, $D(t)$ in Eq.(4.1), should be kept in a reasonable range; the constraints are

given by:

$$L_{min} \leq r(i+k|k) - x(i+k|k) - T\dot{x}(i+k|k) \leq L_{\max}, \tag{4.9}$$

where L_{max} is the maximum following distance. These constraints should be satisfied at each sampling time.

In practice, the future position $r(i+k|k)$ is not exactly known. By assuming that $r(i+k|k)$ is a random variable, we can require the constraints to be satisfied at a given probability α. For example, the minimum safety distance constraint in Eq.(4.9) is rewritten as:

$$P\{r(i+k|k) - x(i+k|k) - T\dot{x}(i+k|k) \leq L_{min}\} \leq 1 - \alpha(\cdot), \tag{4.10}$$

where $\alpha(\cdot)$ is a non-constant value as function of parameters of prediction step i and the acceleration of preceding vehicle $a_r(t)$ discussed in Section 4.2.3. The probabilistic inequality (4.10) can be transformed to the following deterministic inequality:

$$L_{min} + x(i+k|k) + T\dot{x}(i+k|k) \leq r_t^{1-\alpha}(i), \tag{4.11}$$

where $r_t^{1-\alpha}(n)$ is a value at which the cumulative distribution function of position is equal to $1-\alpha$, namely:

$$P\{r(i+k|k) \leq r_t^{1-\alpha}(i)\} = 1 - \alpha$$

Similarly, we can convert the maximum following distance constraint in (4.9) to probability constraints. We will have the following deterministic constraint:

$$r_t^{\beta}(i) - L_{\max} \leq x(i+k|k) + T\dot{x}(i+k|k) \leq r_t^{1-\alpha}(i) - L_{min}, \tag{4.12}$$

where β is a given, satisfying probability value for maximum following distance.

4.2.2.3 Stochastic Prediction of the Position $r(i+k|k)$

For the effective use of the model predictive cruise control, a significant challenges is to predict uncertain future inputs. For immediate predictions ($\approx 0-5s$), this may be done using a Kalman filter and autoregressive moving average algorithms (ARMA). For short term prediction

($\approx 0 - 300s$), prediction with future event information may increase the prediction accuracy. Some examples of future events are: vehicle cut-in, local traffic jams, sudden changes of speed limits, or even road elevation changes. In our discussion, a Markov chain model is developed to predict the uncertainty of the preceding vehicle driving condition over a short horizon and the distribution of the position $r(i+k|k)$ is found through Monte Carlo simulations.

Markov chain Monte Carlo (MCMC) is a powerful means for generating random samples that can be used in computing statistical estimates [68]. References [32,44,59] introduce the Markov chain construction methods for velocity, acceleration, and driver's power demand transition in the application of energy management of hybrid electric vehicles. In our discussion, we only consider the velocity transition of the lead car and exclude the acceleration as a stochastic process assuming the velocity at a next step only depends on its previous step. Another option is to combine the velocity and acceleration as the transition state and construct the Markov chain. However, this method would require a large amount of training data and is unrealistic for this preliminary study.

The transition probability matrix is a square matrix, $P_{N_v \times N_v}$, trained from historical driving data, where N_v is the number of the discretized points for the velocity. The one step transition probability from any state, indexed as m, to another state, indexed as n, is $P_{m,n}$. For multiple e.g. i step transition, the transition matrix is calculated as $P_i = P^i$.

With known state transition probability and current state value, the probability distribution of the future position over the prediction horizon can be calculated using Monte Carlo simulations. Monte Carlo methods are a class of computational algorithms that rely on simulated random sampling to compute their results. Specifically, in our problem, different possible realizations, usually called scenario tree [67], of the velocity $v_r(i+k|k)$ of preceding car are simulated according to the Markov chain transition matrix. The vehicle position is the integral of the velocity and it has the following form in discrete space:

$$r(i+k|k) = r(k) + \frac{1}{2}\sum_{i=0}^{n-1}(v_r(i+k|k) + v_r(i+1+k|k))\Delta t(i),$$

where $\Delta t(i)$ is the sampling time at i step prediction.

The distribution of $r(i+k|k)$ is approximated from the simulation of a large size of pseudo-random numbers using the Metropolis-Hastings algorithm [68]. Monte Carlo simulation generally takes substantial computation time but this work may be done off-line in a real application.

4.2.2.4 Predictive control with prescient information and passive control with state feedback

We compare the results of predictive car following with stochastic preview information to two other cases:

1) Predictive control with precise prescient information

With precise prescient information of the car ahead, $r(i+k|k)$ in Eq. (4.9) is assumed to be exactly known. This is non-causal, but the performance with this level of preview is expected as the benchmark: the best performance that the controller can achieve. The simulation results later shown coincide with this expectation.

2) Passive following model

In a passive following model, the car behind follows the preceding without any knowledge of future driving conditions and a safety following distance is maintained. This is done by a feedback control law $u(t) = k_1\Delta v + k_2\Delta s - k_3\frac{\Delta v^2}{2\Delta s}(\Delta v < 0) + k_4$, where $\Delta v = v_r(t) - v(t), \Delta s = r(t) - x(t) - T\dot{x}(t) - L_{min}$, and k_1, k_2, k_3, k_4 are coefficients as function of Δv. More details about passive following methods may be found in [56].

4.2.3 Case Study and Result Analysis

4.2.3.1 Pre-setting of simulation data

The proposed strategies are evaluated through two driving cycles shown in Fig. 4.4 obtained by driving a vehicle from Clemson, South Carolina to Highland North Carolina with the same driver. The data was obtained from a Garmin GPS 20x receiver with a sampling time of 1 second. In stochastic MPC, the probability of state transition matrix P is trained from the first driving cycle and the MPC with the same P is applied to the two cycles. For the final evaluation of different control strategies, instead of using the cost function J, the fuel economy in miles per gallon(MPG), emissions(CO_2), and tracking distance $D(t)$ are used. With the optimal following velocity calculated using the different control methods, the fuel economy and emissions are computed separately using PSAT. Tracking distance indicates the tracking ability and is expected to stay within a reasonable range.

The probability of the constraint satisfaction, α, has the form $\alpha(\cdot) = \lambda_0\lambda_1^{i-1}$, where i is the prediction step and $\lambda_0 = \lambda_1 = 0.96$. As will be seen later, if we change λ_0 according to the current

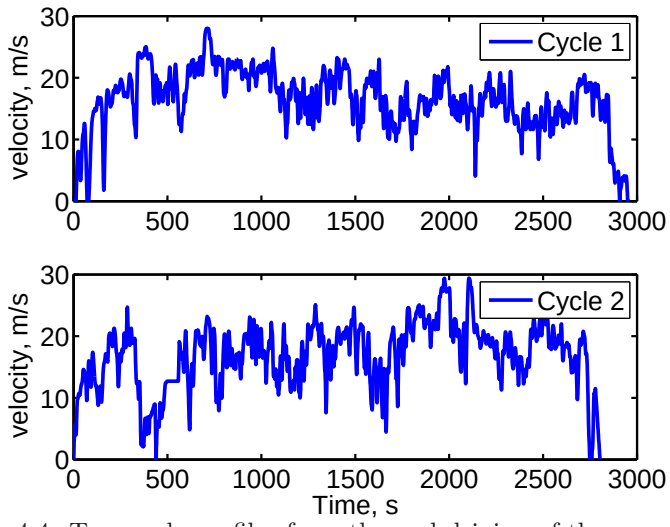

Figure 4.4: Two cycle profiles from the real driving of the same driver

acceleration, better results will be obtained. The setting of β is nearly the same as α; however, β is not adjusted by the acceleration. All other main parameters used in the simulation are listed as follows:

Table 4.1: Simulation parameters

$L_{min}(m)$	$L_{max}(m)$	T(s)	k	N_c	N_p	$\Delta t(i)(s)$
6	200	1.5	0.2	10	10	1

4.2.3.2 Simulation and Analysis

The simulation results of cycle 1 are shown and discussed first followed by that of cycle 2. Fig. 4.4 shows the optimal vehicle velocity from strategies of passive control (P-control), MPC with stochastic input (MPC-STO), and MPC with prescient knowledge (MPC-PRE) and Table 4.2 summarizes the performance including the fuel economy, emissions, and tracking ability. The zoomed figures show that all strategies, like a filter, smooth the velocity trajectory of the following car and the resulting fuel economy improves compared to the leading car. Among the three, the velocity profile from prescient MPC yields the best results for a fuel economy improvement of 32% compared to the leading car. Also, the average tracking distance ($34m$) is less than the stochastic MPC ($48m$) and passive following ($39m$). The excellent performance of MPC with prescient information indicates the improvement margin for other control method. Even though the fuel economy of stochastic MPC(12.1%) is better than that of passive following (11.4%), the larger tracking distance ($48m$) shows that this benefit comes at a performance disadvantage.

By analyzing the stochastic MPC method, the factors contributing to the large following

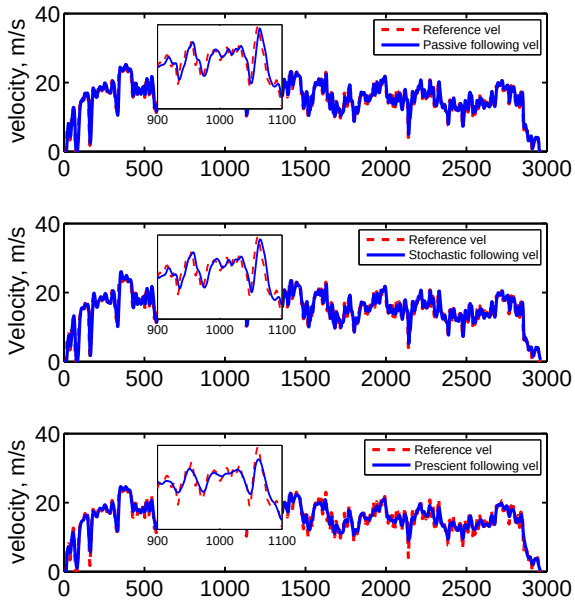

Figure 4.5: Velocity profiles from different control strategies: the first one is from passive control, the second one from MPC with stochastic prediction, and the third one from MPC with prescient driving condition.

distance are found to be the ignorance of acceleration in the probability transition matrix P and a strict setting for α. One option is to add acceleration as an additional state in the transition matrix, however, this will increase the size of P, complicating calculations further and requiring more training data. As an alternative method, we can set the value of α using the current value of acceleration. Specifically, the acceleration of the reference vehicle can be stratified as: hard deceleration, normal deceleration, normal acceleration, or hard acceleration. The value of λ_0 in α is relaxed as $0.96, 0.7, 0.4, 0.2$ depending on the level of acceleration. By doing so, the fuel economy of adjusted MPC-STO can be improved up to 15.5%, the average following distance is reduced to $38m$, and the maximum following distance improves as well.

Table 4.2: Performance comparison of different control methods. 1) P-control: passive control, 2) MPC-PRE:MPC with prescient knowledge of future uncertainty 3) MPC-STO: MPC with prediction of the velocity as a Markov chain

Control method	MPG (normalized)	CO2 (normalized)	E(D(t)), min(D(t)), max(D(t))(m)
Ref. Veh.	1	1	-
P-Control[1)]	1.114	0.89	39.34, 6.00, 71.41
MPC-PRE[2)]	1.320	0.76	34.03, 6.00, 55.52
MPC-STO[3)]	1.121	0.88	48.56, 6.00, 93.32
MPC-STO(adj)[4)]	1.155	0.86	38.30 6.00, 74.34

In above simulations using MPC-STO, the velocity transition matrix P has been trained from cycle 1 itself. As further validation of the proposed MPC-STO control, the same simulations are repeated for cycle 2 while using the transition matrix P trained from cycle 1. These results are

summarized in Table 4.3. To ensure fair comparisons between the performance of MPC-STO and passive following, the parameters in passive following are tuned to match the tracking distance with MPC-STO. The results of these simulations indicate the same findings as seen before for cycle 1.

Table 4.3: Performance comparison for different control methods for cycle 2

Control method	MPG (normalized)	CO2 (normalized)	E(D(t)), min(D(t)), max(D(t))(m)
Reference Veh.	1	1	-
P-Control	1.075	0.93	39.42, 6.00, 73.54
MPC-PRE	1.317	0.76	35.40, 6.00, 57.59
MPC-STO(adj)	1.145	0.87	39.40, 6.00, 84.54

Table 4.4 summarizes all the information required for different control strategies. Passive control needs the least information-current velocity and position of the reference vehicle. MPC-PRE requires the most information-the prescient driving condition for prediction horizon at the beginning of each step. MPC-STO requires only the historical driving information from the reference vehicle.

Table 4.4: Comparison of different control method for the requirement of driving information. $r(t)$:reference vehicle position at current time step t, $v_r(t)$: current reference vehicle velocity, $a_r(t)$:current reference vehicle acceleration, $a_r(\tau), \tau < t$: historical time series acceleration, $a_r(\tau), \tau > t$: (prediction of) future acceleration, P:velocity transition matrix for reference vehicle

Method	Information Requirement					
	$r(t)$	$v_r(t)$	$a_r(t)$	$a_r(\tau)$ $\tau < t$	$v_r(\tau)$ $\tau > t$	P
P-Control	$\surd$	$\surd$	$\times$	$\times$	$\times$	$\times$
MPC-PRE	$\surd$	$\surd$	$\times$	$\times$	$\surd$	$\times$
MPC-STO	$\surd$	$\surd$	$\times$	$\times$	$\times$	$\surd$
MPC-STO(adj)	$\surd$	$\surd$	$\surd$	$\times$	$\times$	$\surd$

We should note that the improvement result strongly depends on the driving cycles and the results will be different for different cycles and vehicles considered. Testing the proposed algorithms with further data from the same driver in general needs further investigation. Also, even though some safety constraints are considered in Eq.(4.9), additional safety constraints could be added if necessary.

4.3 Predictive Control Based on Macroscopic Traffic Information

This part formulates predictive planning of velocity using macroscopic traffic predictions and demonstrates its impacts on fuel economy and emissions of passenger and commercial vehicles via several simulation case studies. We cast the problem as an optimal control problem with the goal of reducing velocity transients while also penalizing trip time. This optimal control problem will be solved numerically by a two dimensional dynamic program. A key to this work is realizing the traffic-imposed constraints on the velocity which requires spatiotemporal estimation of traffic velocity. In this part we focus on highway trips where a longer traffic preview horizon along with coarser traffic information can be effective. For this type of planning knowledge of current state of traffic is not sufficient and a predictive traffic model may be used to estimate the evolving pattern of traffic down the road.

Because a feedfoward traffic estimator that predicts evolution of traffic along the vehicle route is a key part of this work, it is discussed in detail next in Section 4.3.1.1. This is followed by formulation of the optimal velocity planning problem in Section 4.3.1.2. The numerical dynamic programming solution process is described in Section 4.3.1.3. Several simulation case studies are presented in Section 4.3.2.

4.3.1 Methodology

4.3.1.1 Spatiotemporal Prediction of Traffic

There is a vast body of work by traffic engineers, physicists, and computer scientists on traffic modeling. Excellent and thorough review of such models can be found in [27, 50, 51]. Microscopic traffic models use simple car-following rules to model procession and interaction of individual vehicles. These models are described by a system of ordinary differential equations or in the cellular automata approach by rules for advancing individual vehicle in a fine grid in discrete time steps. The drawback of microscopic models is the high computational load as the number of vehicles increases. Macroscopic models use the analogy of traffic flow to fluid flow and formulate spatiotemporal evolution of speed and traffic density using coupled partial differential equations (PDEs). Aggregating a large number of vehicles into a continuum macroscopic model has the advantage of being much

faster computationally. At the same time via macroscopic models it is possible to capture complex traffic phenomena such as a congestion wave, instabilities, and phase transitions of traffic flow [24]. Macroscopic models have also been used for calculating average travel times, fuel consumption and emission levels [55], for short-term forecasts of traffic flow for rerouting [26, 39], and for design of traffic flow control systems [23, 33]. More recently in [20], a gas-kinetic traffic model is used to estimate the future velocity of a plug-in hybrid vehicle. Missing from the literature are methods that help plan the velocity of an individual vehicle to reduce the possibility of its untimely arrival at a local traffic wave.

One way of forming a spatiotemporal traffic map is through these existing gas-kinetic PDE models of traffic to predict its evolution. Specifically in inter-city highway driving use of a predictive model is important due to the long planning horizon. The evolution of average traffic velocity at each point and time $v_t(x,t)$, and average traffic density $\rho_t(x,t)$, are predicted by the following coupled PDEs [27]:

$$\frac{\partial \rho_t}{\partial t} + \frac{\partial(\rho_t v_t)}{\partial x} = q(x,t) \tag{4.13}$$

$$\frac{dv_t}{dt} = \frac{\partial v_t}{\partial t} + v_t \frac{\partial(v_t)}{\partial x} = \frac{v_e(\rho_t) - v_t}{\tau} - \frac{1}{\rho_t}\frac{\partial P}{\partial x} + \frac{\eta}{\rho_t}\frac{\partial^2 v_t}{\partial x^2} \tag{4.14}$$

The first equation describes balance of vehicles; there $q(x,t)$ models the incoming or outgoing traffic at discrete road junctions. The second equation models dynamics of the velocity, characterized by a traffic pressure P expressed as $P = c_0^2 \rho_t$ and traffic viscosity η in which both η and c_0 are constants. The function $v_e(\rho_t)$ captures the speed-density relationship at steady-state. Details on the choice of parameters P and η and the function $v_e(\rho)$ can be found in [24, 35, 47]. Approximate boundary and initial conditions and the ramp inputs $q(x,t)$ can be retrieved from real-time traffic information systems as well as time of the day, season, holidays, current and forecast weather, accidents, or events such as school schedules, sports games and concerts, and even uniquely local variables [13]. The set of coupled PDEs will be solved using a finite-difference approach in real-time to determine traffic-imposed constraints in the future path of a vehicle. For inner-city driving, the *immediate* traffic-imposed bounds on speed can be obtained via infrastructure-to-vehicle communication [31] or via ad-hoc [70, 76] vehicle-to-vehicle communication networks.

4.3.1.2 Optimal Control Problem Setup

The average traffic velocity $v_t(x,t)$ estimated above will be an upper limit to the velocity each vehicle can assume at position x at time t. The goal is to find a velocity profile that i) meets this traffic-imposed speed limit (and the speed limits of the road) and ii) lowers fuel use without too much compromise on trip time. In other words, the slope of each feasible path is upper-bounded by the spatiotemporally varying limit $v_t(x,t)$ imposed by traffic. The problem of finding the optimal speed trajectory $v(x,t)$ can be formalized as an optimal control problem which will be solved numerically. The cost function is:

$$\min_{v(x,t)} J = \int_{x_i}^{x_f} \|L\left(v(x,t)\right)\|_Q^2 \frac{dx}{v(x,t)} \tag{4.15}$$

subject to road speed limits $[v_{min}, v_{max}]$, traffic-imposed bound on speed $v_t(x,t)$, and driver set speed v_{set}:

$$v_{min} \leqslant v(x,t) \leqslant min(v_{max}, v_t(x,t), v_{set}) \tag{4.16}$$

and with acceleration and deceleration constraints imposed on $\dot{v}(x,t)$. In (4.15), x_i and x_f are the origin and destination and $\| \bullet \|_Q$ denotes the weighted 2-norm with the diagonal penalty weighting matrix Q. Appropriate choice of the the integrand $L(v(x,t))$ is an open problem. For example the choice $L(v) = \begin{bmatrix} \dot{m}_f & NO_x & (v(x,t) - v_{set}) \end{bmatrix}^T$ penalizes the fuel rate $\dot{m}_f$ and NO_x emissions, while also penalizing deviations from the driver set speed. The latter ensures travel time is not compromised. Another choice is to explicitly penalize trip time by selecting $L(v) = \begin{bmatrix} \dot{m}_f & NO_x & 1 \end{bmatrix}^T$ which will result in trip time $t_f - t_i$, appearing in the cost function. However inclusion of fuel rate and emissions in the cost function add to the complexity of this optimal control problem, because it requires inclusion of a detailed model of the vehicle powertrain. Therefore in this first investigation we use a simpler form $L(v) = \begin{bmatrix} \dot{v}^2 & 1 \end{bmatrix}^T$ to penalize trip time and velocity transients $\dot{v}$ (accelerations and decelerations) which indirectly contribute to increase in fuel use. This correlation of the cost function with the fuel economy is tested in the simulations with PSAT a commercialized vehicle powertrain simulation software developed by Argonne National Laboratory. Another benefit of using this cost function is that it is independent of a specific powertrain and could be directly transferred among different vehicles. The other factor increasing the fuel use is idling at zero speed; penalizing the total trip time should cut unnecessary idling. The solution $v(x,t)$ can then be issued as a reference to the low-level vehicle controller. Alternatively the velocity $v(x,t)$ can be suggested

to the driver as the eco-friendly speed by a mobile phone or intelligent speed assistant system which has been experimented in Australia and Europe [73]. The PSAT software including a driver model and independent of the optimal control process was used to test the effectiveness of the suggested velocity profile.

4.3.1.3 Numerical Solution Via Dynamic Programming

The optimal control problem posed above cannot be solved analytically due to the spatiotemporally varying constraints imposed on its optimization variables along with several other pointwise-in-time constraints. In this work we solve this problem numerically using a dynamic program.

The vehicle kinematics is represented by the following two-state dynamic equations:

$$\begin{cases} \dot{x} = v \\ \dot{v} = u \end{cases} \tag{4.17}$$

where x and v are position and velocity of the vehicle respectively and u is its acceleration which is selected as a control input. Since the final optimal velocity trajectory is evaluated in powertrain simulation software PSAT, we ignore the the dynamics of the powertrain and driver's reaction time at the upper level control. Therefore $L = \begin{bmatrix} u^2 & 1 \end{bmatrix}^T$ is set in the cost function (4.15). In addition to the velocity constraint (4.16), we impose the acceleration constraint on the input u:

$$a_{\min} \leq u(x,t) \leq a_{\max} \tag{4.18}$$

where $a_{\max}$ is the positive maximum allowable acceleration and $a_{\min}$ is the negative maximum allowable deceleration.

The cost function can be written as follows:

$$J = \int_{x_i}^{x_f} u^2 \frac{dx}{v(x,t)} + \phi(t_f, t_i) \tag{4.19}$$

where $\phi(t_f, t_i)$ is a terminal cost on trip time and proportional to $t_f - t_i$ by a penalty weight.

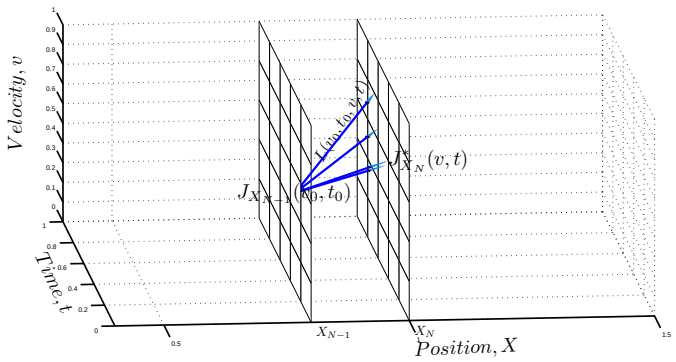

Figure 4.6: Schematic of the DP grid and value function iteration.

The cost function in (4.19) is rewritten in discretized space calculated backward:

$$J = \sum_{n=0}^{N_{\max}} \frac{u^2(x_n, t_{x_n})}{v(x_n, t_{x_n})} \Delta x + \phi(t_f, t_i) \tag{4.20}$$

We also define the the cost function $J_{X_N}(v,t)$ as the cost-to-go from position x_N to the final position which is a function of variables v and t:

$$J_{X_N}(v,t) = \sum_{n=N}^{N_{\max}} \frac{u^2(x_n, t_{x_n})}{v(x_n, t_{x_n})} \Delta x + \phi(t_f, t_i) \tag{4.21}$$

The optimal cost-to-go from position x_N to the final position will then be:

$$J^*_{X_N}(v,t) = \min_u \sum_{n=N}^{N_{\max}} \frac{u^2(x_n, t_{x_n})}{v(x_n, t_{x_n})} \Delta x + \phi(t_f, t_i) \tag{4.22}$$

The optimal acceleration u^* can be found relying on Bellman's optimality principle and by value function iterations backward-in-position as shown in Fig. 4.6. Given the optimal cost-to-go $J^*_{X_N}$ iterations over each node on the planar grid at x_{N-1} will yield the optimal cost-to-go $J^*_{X_{N-1}}$:

$$J^*_{X_{N-1}}(v,t) = \min_{u(x_{N-1})} (J^*_{X_N}(v,t) + \frac{u^2(x_{N-1})}{v(x_{N-1})}) \tag{4.23}$$

and also determines the optimal control $u^*(x_{N-1})$. The process is continued backward-in-position until the sequence of optimal control inputs over the entire trip is determined.

The above solution is a constraint-admissible velocity profile that follows the set target speed as closely as possible. In order to estimate the fuel economy of the vehicle when following this optimal velocity trajectory, a production vehicle is selected and its powertrain model is assembled

from the extensive database of Powertrain System Analysis Toolkit (PSAT).

4.3.2 Simulation Results

For the fuel economy evaluation, two different vehicles have been considered: a passenger vehicle and a mid-size truck. The passenger vehicle is an economy-sized car with 5-speed automatic transmission, 1000 kg mass and 115 hp maximum power. The midsize truck has 6-speed automatic transmission, 8500 kg mass, and 500 hp maximum power. The fuel economy evaluation process is done in PSAT v6.2. In all simulations the maximum acceleration is assumed to be 2 m/s^2 which is a conservative estimate of maximum acceleration capability of a midsize vehicle. Assuming braking on dry asphalt, the friction coefficient of $\mu_b = 0.69$ yields the maximum possible deceleration of 6.7 m/s^2. However, to exclude aggressive driving, maximum braking deceleration of 3 m/s^2 is assumed.

Two simulation case studies were conducted to determine the potential impact on fuel economy and trip time of a vehicle when future state of traffic is available through the model formulated in Section 4.3.1.1. The parameters of the system of partial differential equations 4.13 and 4.14 are summarized in Table 4.5. The resolution of the velocity distribution surface is 900 by 450 which corresponds to 20 meters and 1 second along position and time vectors.

Table 4.5: Macroscopic traffic model parameters

Parameter	Value	Unit
τ	0.01	s
v_f	20	m/s
ρ_{jam}	0.2	$vehicle/m$
α	6000	$1/m$

In order to generate three dimensional spatiotemporal traffic flow surfaces for both backward and forward wave cases, the macroscopic traffic flow governing equations (system of PDEs in equations 4.13 and 4.14) need to be provided with a set of boundary and initial conditions for each case. Two sets of boundary and initial conditions have been assumed such that upstream, downstream and initial steady speed of traffic flow are 18 m/s and 10 m/s for forward and backward waves respectively. To create a transient congestion wave, a ramp input flow $q(x,t)$ is injected into equation (4.13) and represents a flow of cars entering the road from a side ramp. Here we assume the ramp is at position 3200 m and the ramp input is only nonzero during the time interval $[100, 200]$. In this time interval we assume two constant flow rates of 0.022 and 0.024 vehicle/m/s which result

in forward and backward congestion waves respectively.

Given the traffic flow information calculated above, the vehicle velocity is calculated by solving numerically the optimal control problem posed in Section 4.3.1.2 . The results are compared to those of the conventional vehicle which is expected to move with the traffic stream. In other words, a conventional vehicle trajectory moves on the solution surface of Figure 4.7 or 4.8.

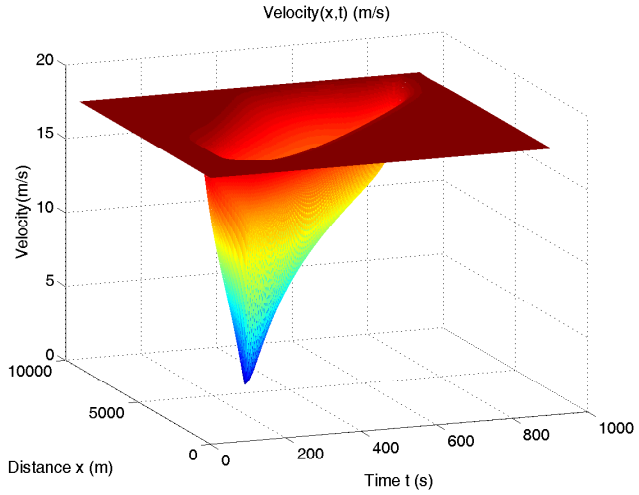

Figure 4.7: Generated spatiotemporal traffic flow surface for a forward congestion wave.

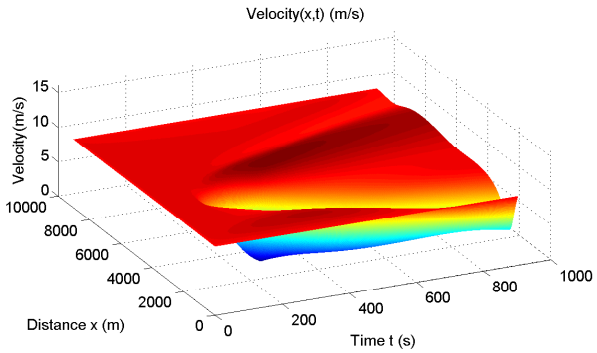

Figure 4.8: Generated spatiotemporal traffic flow surface for a backward congestion wave.

Tables 4.6 and 4.7 summarize the statistics of the resulting velocity profiles of conventional and preview vehicles for forward and backward congestion wave cases respectively. Also shown is the fuel economy when following these trajectories, calculated for a passenger and a midsize heavy vehicle. The results show that in forward congestion waves, up to 12 percent fuel saving for a passenger vehicle and 8 percent fuel saving for the heavy vehicle is obtained when the traffic information is predictively utilized. The savings are less in backward congestion wave. In all cases there is a compromise on trip time.

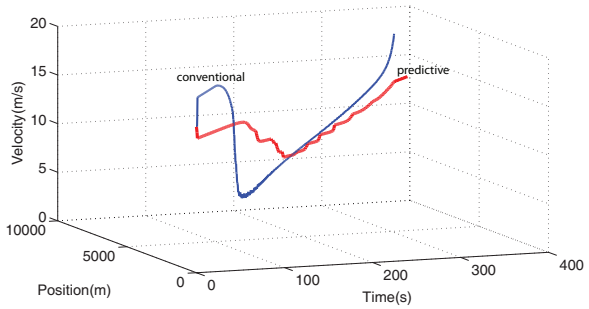

Figure 4.9: Trajectory of the vehicle with and without preview when faced with the forward traffic wave.

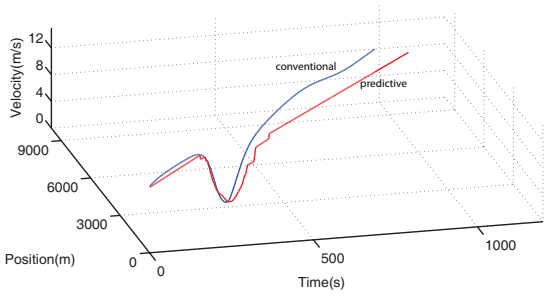

Figure 4.10: Trajectory of the vehicle with and without preview when faced with the backward traffic wave.

Table 4.6: Conventional and preview vehicles in the forward congestion wave.

	Conventional	Preview	Unit
Max. Velocity	18.0	15.0	m/s
Min. Velocity	8.4	5.1	m/s
Trip Time	735	765	s
Fuel Economy (Passenger Vehicle)	49.26	55.00	mpg
Fuel Economy (Heavy Vehicle)	7.04	7.93	mpg

Table 4.7: Conventional and preview vehicles in the backward congestion wave.

	Conventional	Preview	Unit
Max. Velocity	11.7	10.0	m/s
Min. Velocity	1.8	1.8	m/s
Trip Time	956	1058	s
Fuel Economy (Passenger Vehicle)	54.20	56.10	mpg
Fuel Economy (Heavy Vehicle)	7.97	8.07	mpg

4.4 Conclusion

In this chapter, we propose to utilize the traffic flow information in conventional vehicles for predictive adaptive control and route velocity planning. The traffic flow prediction is classified

into three levels, namely, microscopic level, mesoscopic level, and macroscopic level based on the time-scale of varying and the importance to the driver.

In a microscopic level, an adaptive cruise control system has been formulated using the model predictive control framework with probabilistic gap constraints on the separation distance to a leading vehicle. Solution of this problem required velocity prediction of the front car, which was done using a Markov chain assumption for the velocity transients. The probability distribution of the velocity over the prediction horizon was calculated using Monte Carlo simulations. This allowed the conversion of the chance constrained MPC problem into a deterministic problem. The resulting controller was tested in two case studies based on experimental data which demonstrated improvement in fuel economy as compared to a passive car following model.

This chapter also investigates the prediction of macroscopic traffic information with gas-kinetic traffic models. It was assumed that future state of traffic in space and time can be estimated and used as an spatiotemporal upper bound on how fast a vehicle can travel. One possible method for estimation of velocity proposed in this work is using real-time traffic information as initial conditions to a macroscopic traffic model represented by a set of coupled nonlinear partial differential equations. An optimal control problem was cast with the estimated traffic flow surface as the upper bound on the velocity and with the target of improving fuel economy. The validity of the approach was investigated in two different simulation case studies in which the PDE traffic model was solved to generate the traffic surface. The fuel evaluation simulations showed up to 12 percent improvement of fuel economy was possible when the future state of traffic was known. This improvement was achieved at the cost of 4 to 10 percent increase in trip time. The simulations also showed that traffic preview may be more beneficial to fuel economy when the traffic congestion moves "forward" in space. The suggested reference velocity could be shown in an add-on accessory such as a smart phone or used in intelligent speed assistant systems.

The predictive control with mesoscopic information including terrain and traffic light prediction is not discussed in this work and could be found in [4, 49, 25, 29]. A future work may be on the integration of different level predictions together in predictive cruise control (PCC) systems.

Chapter 5

Summary of Contributions and the Future Work

5.1 Novel Contributions

The contribution of this dissertation is the application of optimal control in three areas of technology: hybrid electric, plug-in hybrid, and conventional vehicles based on different types of preview information. More specifically the contributions in each chapter are:

In chapter 2 , the fuel efficiency improvement through previewing future 3D terrain maps in power management of hybrid electric vehicle was quantified. We

1. Investigated, for the first time, fuel economy benefit of previewing 3D terrain by employing optimal control methods ECMS and DP.

2. Proposed different baseline strategies without any future information and concluded that the improvement is baseline dependent.

3. Studied the benefit of preview for reducing energy flow from and to the battery which relates to life cycle of the battery.

In chapter 3, the fuel economy benefit of partial or full preview of future driving conditions in plug-in hybrid electric vehicles was investigated by applying optimal control in a systematic manner. We

1. Proposed a novel combination of standard ECMS strategy and a backward ECMS or DP strategy to handle partial preview information in the energy management of a PHEV.

2. Quantified the fuel economy benefit attainable by different preview levels and evaluated its sensitivity to preview levels.

3. Demonstrated reduction in online computations which is important for optimal use of preview information in real-time.

In chapter 4, we studied how traffic flow information and prediction can help fuel savings and emission reduction in passenger and commercial vehicles. We

1. Proposed a multiscale preview and optimal control structure to integrate macroscopic and microscopic traffic information for fuel saving and emission reduction by optimal velocity planning.

2. Introduced a stochastic framework for modeling the uncertainty of vehicle velocity in the microscopic traffic level; applied a stochastic model predictive control method in vehicle's adaptive cruise control systems.

3. Proposed the use of a gas-kinetic traffic models for predicting the macroscopic traffic flow evolution, which fed a nonlinear programming (two-dimension dynamic programming) algorithm for vehicle's velocity planning as the driver's reference velocity.

4. Quantified the fuel economy and emission benefit attainable by previewing microscopic and macroscopic traffic information.

5.2 Future Work

We used different kinds of future information including road terrain, trip distance, traffic flow in energy management of hybrid electric vehicles, plug-in hybrid electric vehicles, and conventional vehicles and showed noticeable benefit of predictive control for fuel consumption and emission reduction. However, there is more room for enhancing the proposed methods in different applications for extending this work. Several directions for future research are suggested below:

1. A real-time implementable algorithm for terrain preview based energy management of HEVs:

In chapter 2, we investigated the value of the 3D road terrain in improving the energy management of an HEV with constant cruise speeds. However, the assumption of constant speed limits its real-time implementation. To deal with the uncertainty of the velocity, the methodologies proposed in chapter 3 with preview information for the energy management of PHEVs can be transferred or adapted for HEVs. Three different methods were proposed to estimate the optimal operation parameter (s or λ), namely, D-ECMS, E-ECMS, and B-ECMS. The first two (D-ECMS and E-ECMS) methods for estimating the equivalent factor are directly transferable for HEVs if the preview of road terrain and trip velocity is assumed. Moreover, the proposed B-ECMS approach can be utilized for incorporating terrain preview.

The available regeneration energy of an HEV resulting from the elevation change could be estimated assuming a fixed length prediction horizon. The length of prediction horizon needs to be optimized for different HEV configurations and system specifications. The estimated regeneration energy can be converted to a net change of the batter's state-of-charge (NCSOC). The SOC to determine the equivalent factor can be adjusted by subtracting the NCSOC from the real SOC. The equivalent factor s can still be found through the look-up map shown in Fig. 2.6. The preview process will be carried out in a moving horizon manner and can be updated at each step. Since the value of s is updated according to a pre-defined table not accounting for the velocity, the prediction of the velocity is not necessary and the computation burden is reduced significantly enabling efficient online use. By doing so, the regeneration energy is used predictively and optimally.

2. Further investigating data-based prediction methods for microscopic traffic information preview:

   In chapter 4, we investigated a data-based model by stochastic modeling. There exists other data-based methods as prediction tools including ARMA(autoregressive moving average) and artificial neural network (ANN) model by predicting the vehicle velocity based on historical data. In connected vehicles, where the vehicle in the network is supposed to share its instantaneous data with neighboring vehicles, the prediction of the lead vehicle's movement could be done by utilizing all available (historic) data from the networked vehicles.

3. Developing event-based traffic flow prediction models:

   Prediction of traffic events can enhance prediction of traffic flow. Among various events, traffic

light status is one of the most critical ones to traffic flow and can be predicted given traffic light triggering logics and real-time and historic traffic information. Recurrent traffic jams, can be predicted based on historic data. Topographical information such as a downstream road curve reduces the traffic speed and could also be thought of as an event.

4. Integration of different level control and preview:

   We proposed to use predictive control and preview of traffic flow information in different levels. The predictive control with microscopic information was proposed for adaptive cruise control systems and that with macroscopic prediction was used to generate the reference velocity for drivers. In the future work, we propose to combine these different levels of information together. A high level layer predicts the macroscopic or mesoscopic traffic evolution trend and plans the vehicle route velocity; a low planning level predicts the mesoscopic or microscopic traffic condition and applies the predictive adaptive control according to instantaneously updated vehicle states.

5.3 Dissemination of Results

Journal

- ☐ Chen Zhang, Ardalan Vahidi, "Route preview in energy management of plug-in hybrid electric vehicle", accepted for publication in IEEE Transaction on Control Systems Technology.
- ☐ Chen Zhang, Ardalan Vahidi, Pierluigi Pisu, Xiaopeng Li, and Keith Tennant, "Role of terrain preview in energy management of hybrid electric vehicles", in IEEE Transactions on Vehicular Technology, Vol.59, No.3, Pages 1139-1147, 2010.

Conference

- ☐ Chen Zhang, Ardalan Vahidi, "Model predictive cruise control with probabilistic constraints for eco-driving", submitted to 2011 American Control Conference (ACC), 2011
- ☐ Ali Borhan, Chen Zhang, Ardalan Vahidi, "Nonlinear model predictive control for power-split hybrid electric vehicles", in Proceedings of the 49th IEEE Conference on Decision and Control, Atlanta, Georgia, 2010.
- ☐ Behrang Asadi, Chen Zhang, Ardalan Vahidi, "The potential of traffic flow preview for planning fuel optimal vehicle velocity", in Proceedings of the 3rd Annual Dynamic Systems and Control Conference (DSCC), Cambridge, Massachusetts, 2010.
- ☐ Chen Zhang, Ardalan Vahidi, "Real-time optimal control of plug-in hybrid vehicles with trip preview", in Proceedings of 2010 American Control Conference, Baltimore, Maryland, 2010.
- ☐ Chen Zhang, Ardalan Vahidi, Xiaopeng Li, Dean Essenmacher,"Role of trip information preview in fuel economy of plug-in hybrid vehicles", in Proceedings of ASME Dynamic System Control Conference, Los Angeles, California, 2009.
- ☐ Chen Zhang, Ardalan Vahidi, Xiaopeng Li, Tennant Keith,"Utilizing road grade preview for increasing fuel economy of hybrid vehicles", in Proceedings of Control in Transportation Systems of IFAC 2009, Long Beach, California, 2009.

Bibliography

[1] Connected vehicle testing begins at MIS. Web. http://www.mispeedway.com/Articles/2009/08/Connected-vehicle-testing.aspx.

[2] Mobile Millennium Project. Web. http://traffic.berkeley.edu, link retrieved on July 6, 2009.

[3] B. Asadi and A. Vahidi. Predictive use of traffic signal state for fuel saving. *Proceedings of 12th IFAC Symposium on Transportation Systems*, pages 484–489, 2009.

[4] B. Asadi and A. Vahidi. Predictive cruise control:utilizing upcoming traffic signal information for improving fuel economy and reducing trip time. *IEEE Transactions on Control Systems Technology*, pp(99):1–9, 2010.

[5] Jonn Axsen and Ken Kurani. The early U.S. market for PHEVs: Anticipating consumer awareness, recharge potential, design priorities and energy impacts. Aug. 2008. http://pubs.its.ucdavis.edu/publication_detail.php?id=1191.

[6] V.L. Bageshwar, W.L. Garrard, and R. Rajamani. Model predictive control of transitional maneuvers for adaptive cruise control vehicles. *IEEE Transactions on Vehicular Technology*, 53(5):1573–1585, Sep. 2004.

[7] Dimitri P. Bertsekas. *Dynamic Programming and Optimal Control*. Athena Scientific, 2007.

[8] Authur E. Bryson and Yu-Chi Ho. *Applied Optimal Control*. Taylor Francis, 1975, pp.4-9.

[9] D. L. Buntin and J. W. Howze. A switching logic controller for a hybrid electric/ICE vehicle. *Proceedings of of American Control Conference, Seattle, WA*, Jun. 1995.

[10] Andrew Burke and Eric Van Gelder. Plug-in hybrid-electric vehicle powertrain design and control strategy options and simulation results with lithium-ion batteries. Mar. 2008. http://phev.ucdavis.edu/publications/pubs/EET-08paper%20formatted3.pdf.

[11] Karen L. Butler, Mehrdad Ehsani, and Preyas Kamath. A Matlab-based modeling and simulation package for electric and hybrid electric vehicle design. *IEEE Transaction on Vehicular Technology*, 48(6):1770–1778, Nov. 1999.

[12] D. Caveney. Cooperative vehicular safety applications. *IEEE Control Systems Magazine*, 30(4):38 –53, Aug. 2010.

[13] INRIX Company. Innovative technologies: INRIX dynamic predicitive traffic.

[14] S. Delprat, T.M. Guerra, and J. Rimaux. Control strategies for hybrid vehicles: Optimal control. *IEEE 56th Vehicular Technology Conference*, 3:1681–1685, Sept. 2002.

[15] S Delprat, T.M. Guerra, and J Rimaux. Control strategies for hybrid vehicles: Synthesis and evaluation. *Vehicular Technology Conference, 2003. VTC 2003-Fall. 2003 IEEE 58th*, 5:3246–3250, Oct. 2003.

[16] Department of Energy (DOE). http://www.energy.gov/pricestrends/index.htm.

[17] Environmental Protection Agency. http://www.epa.gov/fueleconomy/label/nprm-label2010.pdf.

[18] Lawrence C. Evans. *An Introduction to Stochastic Differential Equations*. UC Berkeley, 2006. http://math.berkeley.edu/~evans/SDE.course.pdf.

[19] Qiuming Gong, Yaoyu Li, and Zhong-Ren Peng. Trip-based optimal power management of plug-in hybrid electric vehicles. *IEEE Transaction on Vehicular Technology*, 57(6):3393–3401, Nov. 2008.

[20] Qiuming Gong, Yaoyu Li, and Zhongren Peng. Trip based optimal power management of plug-in hybrid electric vehicles using gas-kinetic traffic flow model. *Proceedings of the American Control Conference*, 2008.

[21] Qiuming Gong, Yaoyu Li, and Zhongren Peng. Power management of plug-in hybrid electric vehicles using neural network based trip modeling. *Proceedings of the American Control Conference*, 2009.

[22] L. Guzzella and A. Sciarretta. *Vehicle Propusion Systems: Introduction to Modeling and Opitmization*. Springer, 2005.

[23] A. Hegyi, B. De Schutter, and H. Hellendoorn. Model predictive control for optimal coordination of ramp metering and variable speed limits. *Transportation Research Part C: Emerging Technologies*, 13(3):185–209, 2005.

[24] D. Helbing and M. Treiber. Gas-kinetic-based traffic model explaining observed hysteretic phase transition. *Physical Review Letters*, 81(14):3042–345, 1998.

[25] Erik Hellstrm, Maria Ivarsson, Jan slund, and Lars Nielsen. Look-ahead control for heavy trucks to minimize trip time and fuel consumption. *Control Engineering Practice*, 17(2):245–254, 2009.

[26] M. Hilliges and W. Weidlich. A phenomenological model for dynamic traffic flow in networks. *Transportation Research-Part B*, 29:407–431, 1995.

[27] S. Hoogendoom and P. Bovy. State-of-the-art of vehicular traffic flow modelling. *Proceedings of the Institution of Mechanical Engineers, Part I: Journal of Systems and Control Engineering*, 215(4):283–303, 2001.

[28] Li hua Luo, Hong Liu, Ping Li, and Hui Wang. Model predictive control for adaptive cruise control with multi-objectives: comfort, fuel-economy, safety and car-following. *Joural of Zhejiang Univ-Sci A*, 11(3):191–201, 2010.

[29] Wei Huang, David M. Bevly, Xiaopeng Li, and Steve Schnick. 3D road geometry based optimal truck fuel economy. *Proceedings of ASME Int. Mechianical Engineering Congfress and Exposition*, Nov. 2007.

[30] Ricardo Inc. Impact of vehicle weight reduction on fuel economy for various vehicle architectures. Technical report, 2008. `http://aluminumintransportation.org/downloads/AluminumNow/Ricardo 20Study_with 20cover.pdf`.

[31] D. Jiang, V. Taliwal, A. Meier, W. Holfelder, and R. Herrtwich. Design of 5.9 GHz DSRC-based vehicular safety communication. *IEEE Wireless Communications*, 13:36–43, 2006.

[32] Lars Johannesson, Mattias Åsbogård, and Bo Egardt. Assessing the potential of predictive control for hybrid vehicle powertrains using stochastic dynamic programming. *Proceedings of IEEE Conference on Intelligent Transportation Systems*, pages 366–371, 2005.

[33] A. Karimi, A. Hegyi, B. De Schutter, H. Hellendoorn, and F. Middelham. Integration of dynamic route guidance and freeway ramp metering using model predictive control. *Proceedings of the American Control Conference*, 6:5533–5538, June-July 2004.

[34] S. Kato, S. Tsugawa, K. Tokuda, T. Matsui, and H. Fujii. Vehicle control algorithms for cooperative driving with automated vehicles and intervehicle communications. *IEEE Transactions on Intelligent Transportation Systems*, 3(3):155–161, Sep. 2002.

[35] B.S. Kerner, P. Konhaüser, and M. Schilke. A new approach to problems of traffic flow theory. *Proceedings of the 13th International Symposium on Transportation and Traffic Theory*, 1996.

[36] T.-S. Kim, C. Manzie, and H. Watson. Fuel economoy benefits of look-ahead capability in a mild hybrid configuration. *Proceedings of the 17th IFAC World Congress*, pages 5646–5651, 2008.

[37] A. Kleimaier and D. Schröder. An approach for the online optimized control of a hybrid powertrain. *Proceedings of 7th International Workshop on Advanced Motion Control*, pages 215–220, 2002.

[38] Nicholas J. Kohut, J. Karl Hedrick, and Francesco Borrelli. Integrating traffic data and model predictive control to improve fuel economy. In *the 12th International IEEE Conference on Intelligent Transportation Systems, 2009. ITSC '09.*, pages 155–160, Oct. 2009.

[39] R. D. Kühne, K. Langbein-Euchner, M. Hilliges, and N. Koch. Evaluation of compliance rates and travel time calculation for automatic alternative route guidance systems on freeways. *Transportation Research Record*, 1554:153–161, 1996.

[40] Argonne National Laboratory. Powertrain System Analysis Toolkit. Commercial Software. `http://www.transportation.anl.gov/software/PSAT/index.html`.

[41] L. Li, Fei-Yue Wang, and H. Kim. Cooperative driving and lane changing at blind crossings. In *Proceedings of IEEE Intelligent Vehicles Symposium, 2005.*, pages 435–440, Jun. 2005.

[42] Shengbo Li, Keqiang Li, R. Rajamani, and J. Wang. Multi-objective coordinated control for advanced adaptive cruise control system. In *Proceedings of the 48th IEEE Conference on Decision and Control, held jointly with the 2009 28th Chinese Control Conference. CDC/CCC 2009.*, pages 3539 –3544, Dec. 2009.

[43] C.-C Lin, H. Peng, J. Grizzle, and J.-M. Kang. Power management strategy for a parallel hybrid electric vehicle. *IEEE Transactions On Control Systems Technology*, 11(6), 2003.

[44] Chan-Chiao Lin, Huei Peng, and J.W. Grizzle. A stochastic control strategy for hybrid electric vehicles. In *Proceedings of the 2004 American Control Conference.*, volume 5, pages 4710–4715, Jun. 2004.

[45] Jinming Liu, Huei Peng, and Z. Filipi. Modeling and control analysis of Toyota hybrid system. In *Advanced Intelligent Mechatronics. Proceedings, 2005 IEEE/ASME International Conference on*, pages 134–139, 2005.

[46] Xiao-Yun Lu, Pravin Varaiya, Roberto Horowitz, and Joe Palen. Faulty loop data ananlysis/correction and loop faulty detection. `http://www.me.berkeley.edu/ horowitz/Publications_files/All_papers_numbered /172C_Lu_Loop_Fault_Final_Ver.pdf`.

[47] A.D. Lyrintzis, G. Liu, and P.G. Michalopoulos. Development and comparative evaluation of high-order traffic flow models. *Transportation Research Record*, 1547:174–183, 1994.

[48] Hani S. Mahmassani, Jing Dong, Jiwon Kim, and Roger B. Chen. Incorporating weather impacts in traffic estimation and prediction systems. *ITS Report*, Sept. 2009. `http://ntl.bts.gov/lib/31000/31400/31419/14497.htm`.

[49] S. Mandava, K. Boriboonsomsin, and M. Barth. Arterial velocity planning based on traffic signal information under light traffic conditions. In *the 12th International IEEE Conference on Intelligent Transportation Systems, 2009. ITSC '09.*, pages 1–6, Oct. 2009.

[50] K. Nagel. Particle hopping models and traffic flow theory. *Physical Review E.*, 53(5):4655, 1996.

[51] K. Nagel, P. Wagner, and R. Woesler. Still flowing: Approaches to traffic flow and traffic jam modeling. *Operations Research*, 51(5):681–710, 2003.

[52] National Highway Traffic Safety Administration. http://www.nhtsa.gov/staticfiles/rulemaking/pdf/cafe/2017+CAFE_and_GHG_Notice_of_Intent.pdf.

[53] G. Paganelli, S. Delprat, T.M. Guerra, J. Rimaux, and J.J. Santin. Equivalent consumption minimization strategy for parallel hybrid powertrains. *Vehicular Technology Conference*, 4:2076–2081, 2002.

[54] G. Paganelli, Y. Guezennec, and G. Rizzoni. Optimizing control strategy for hybrid fuel cell vehicle. *SAE*, 2002-0102, 2002, Warrendale, PA, Tech. Rep.

[55] H. J. Payne. FREFLO: A macroscopic simulation model of freeway traffic. *Transportation Research Record*, 68, 1979.

[56] M. Persson, F. Botling, E. Hesslow, and R. Johansson. Stop and go controller for adaptive cruise control. In *Proceedings of the 1999 IEEE International Conference on Control Applications*, volume 2, pages 1692–1697, 1999.

[57] Pierluigi Pisu and Giorgio Rizzoni. A comparative study of supervisory control strategies for hybrid electric vehicle. *IEEE Transactions On Control Systems Technology*, 15(3), May 2007.

[58] Research and Innovative Technology Administration of U.S. Department of Transportation (DOT). IntelliDrive, 2010. http://www.intellidriveusa.org.

[59] G. Ripaccioli, Daniele Bernardini, Stefano Di Cairano, Alberto Bemporad, and Ilya V. Kolmanovsky. A stochastic model predictive control approach for series hybrid electric vehicle power management. In *Proceedings of 2010 American Control Conference*, pages 5844–5899, Jun. 2010.

[60] G. Rizzoni, P. Pisu, and E. Calo. Control strategies for parallel hybrid electric vehicles. *Proceedings of IFAC Symposium on Advanced Automotive Control*, pages 508–513, 2004.

[61] Dean Rotenberg, Ardalan Vahidi, and Ilya Kolmanovsky. "Ultracapacitor Assisted Powertrains: Modeling, Control, Sizing, and the Impact on fuel economy". In *2008 American Control Conference*, pages 981–987, Seattle, Washington, USA, Jun. 2008.

[62] A. Rousseau. PHEV vehicle level control strategy summary. Nov. 2008. http://www.transportation.anl.gov/pdfs/HV/552.pdf.

[63] M. Salman, M.-F. Chang, and J.-S. Chen. Predictive energy management strategies for hybrid vehicles. *Proceedings of IEEE Vehicle Power and Propulsion Conference*, pages 21–25, 2005.

[64] A. Sciarretta, L. Guzzella, and M. Back. A real-time optimal control strategy for parallel hybrid vehicles with on-board estimation of control parameters. *Proceedings of IFAC Symposium Advances in Automotive Control*, pages 502–507, 2004.

[65] Antonio Sciarretta, Michael Back, and Lino Guzzella. Optimal control of parallel hybrid electric vehicles. *IEEE Transactions On Control Systems Technology*, 12(3), May 2004.

[66] Antonio Sciarretta and Lino Guzzella. Control of Hybrid Electric Vehiciels. *IEEE Control System Magazine*, pages 60–67, Apr. 2007.

[67] Alexander Shapiro, Darinka Dentcheva, and Andrzej Ruszczyski. *Lectures on Stochastic Programming: Modeling and Theory*. SIAM-Society for Industrial and Applied Mathematics, Sept. 2009.

[68] J.C. Spall. Estimation via Markov chain Monte Carlo. *Control Systems Magazine, IEEE*, 23(2):34–45, Apr. 2003.

[69] Robert F. Stengel. *Optimal Control and Estimation*. Dover, pages 204-207, 1994.

[70] Z. Ting, X. Bo, and O. Wolfson. Disseminating real-time traffic information in vehicular ad-hoc networks. *Proceedings of IEEE Intelligent Vehicle Symposium*, pages 1056–1061, 2008.

[71] Pinak Tulpule, Stephanie Stockar, Vincenzo Marano, and Giorgio Rizzoni. Optimality assessment of equivalent consumption minimization strategy for phev applicaiton. *Proceedings of the ASME 2009 Dynamic Systems and Control Conference*, 2009.

[72] U.S. Deparment of Energy. *Transportation Energy Data Book*. `http://www-cta.ornl.gov/data/index.shtml`.

[73] S. Vlassenroot, J. Willem van der Pas, J. De Mol, V. Marchau, K. Brookhuis, and G. Allaert. Speed management through vehicle measures, intelligent transport systems and intelligent speed assistance. 2005. `http://www.shlow.eu/documents/shlow-camp/8ITSandISA.pdf`.

[74] Keith B. Wipke, Matthew R. Cuddy, and Steven D. Burch. A user-friendly advanced powertrain simulation using a combined backward/forward approach. *IEEE Transaction on Vehicular Technology*, 48(6):1761, Nov. 1999.

[75] D.B. Work, O.-P. Tossavainen, S. Blandin, A.M. Bayen, T. Iwuchukwu, and K. Tracton. An ensemble Kalman filtering approach to highway traffic estimation using GPS enabled mobile devices. In *the 47th IEEE Conference on Decision and Control (CDC), 2008.*, pages 5062–5068, Dec. 2008.

[76] C.-Y. Ya, C.-M. Chen, P.-Y. Lin, and S.-L. Tsao. A real-time road traffic information system based on a peer-to-peer approach. *Proceedings of IEEE Symposium on Computers and Communications*, pages 513–518, 2008.

[77] Chen Zhang, A. Vahidi, Xiaopeng Li, and Dean Essenmacher. Role of trip information preview in fuel economy of plug-in hybrid vehicles. *Proceedings of 2009 ASME Dynamic Systems and Control Conference*, 2009.

[78] Chen Zhang, A. Vahidi, P. Pisu, Xiaopeng Li, and K. Tennant. Role of terrain preview in energy management of hybrid electric vehicles. *IEEE Transactions on Vehicular Technology*, 59(3):1139–1147, Mar. 2010.

[79] Chen Zhang, A. Vahidi, Pierluigi Pisu, Xiaopeng Li, and Keith Tennant. Utilizing road grade preview for increasing fuel economy of hybrid vehicles. *Proceedings of 2009 CTS of IFAC*, 2009.

[80] Chen Zhang and Ardalan Vahidi. Route preview in energy management of plug-in hybrid electric vehicles. *Accepted by IEEE Transactions on Control Systems Technology.*

[81] J. Zhang and P.A. Ioannou. Longitudinal control of heavy trucks in mixed traffic: environmental and fuel economy considerations. *IEEE Transactions on Intelligent Transportation Systems*, 7(1):92–104, Mar. 2006.

Appendix

Influence of the Parameter Variation on Optimality of Constant Equivalent Factor in a PHEV

In the following discussion, we study how variation of open circuit voltage V_{oc} of the battery impacts the optimality of a constant equivalent factor. Battery resistance R, and capacitance C, are assumed to be constants. Recall Eq. (3.8):

$$\dot{\lambda}(t) = \frac{-\partial H(SOC, \mathrm{u}, \mathrm{t})}{\partial SOC} = -\lambda(t)\frac{\partial \dot{SOC}}{\partial SOC}$$

Taking partial derivative of Eq. (3.1) with respect to SOC and defining $P_{max} = \frac{V_{oc}^2}{4R}$ yield:

$$\frac{\partial \dot{SOC}}{\partial SOC} = \frac{1}{2RC}(-1 + \frac{1}{\sqrt{1 - P_{batt}/P_{\max}}})\frac{\partial V_{oc}}{\partial SOC} \tag{1}$$

In our next discussion, we assume that $\frac{P_{batt}}{P_{max}} \ll 1$. For example, in the lithium-ion battery package assumed in this work, the internal resistance is around $0.1-0.15\Omega$ (data from PSAT) and the voltage is around $270V$. Then $P_{\max} = \frac{V_{oc}^2}{4R} = \frac{270^2}{4\times 0.15} = 121500W$. Note that this maximum power is typically larger than the rated maximum power of the battery. The calculated battery operating power for the selected PHEV in highway driving cycle is usually less than $20kW$ and less than $12kW$for a same size HEV. In both cases the assumption of $\frac{P_{batt}}{P_{max}} \ll 1$ is not a bad assumption. Using this assumption and using a Taylor series expansion we can write,

$$\frac{\partial \dot{SOC}}{\partial SOC} \approx \frac{1}{2RC}(-1 + 1 + \frac{2P_{batt}R}{V_{oc}^2})\frac{\partial V_{oc}}{\partial SOC} = \frac{P_{batt}}{V_{oc}^2 C}\frac{\partial V_{oc}}{\partial SOC} \tag{2}$$

The relationship between V_{oc} and SOC can be approximated by an exponential function fitted to the experimental data available in the PSAT database (see the following figure). Therefore:

$$\frac{\partial V_{oc}}{\partial SOC} = C_1 V_{oc}, \tag{3}$$

where C_1 is a constant. Substituting Eq. (3) into Eq. (2) yields

$$\frac{\partial \dot{SOC}}{\partial SOC} \approx \frac{C_1 P_{batt}}{V_{oc} C} \tag{4}$$

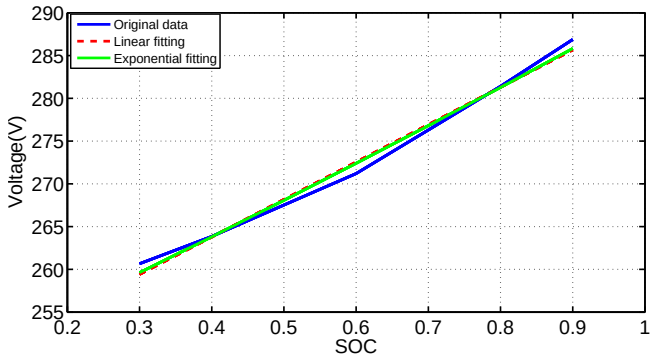

Figure 1: Comparison of different fitting methods-linear fitting and exponential fitting for battery open circuit voltage V_{oc}

Then the co-state dynamics becomes:

$$\dot{\lambda}(t) \approx -\lambda(t)\frac{C_1 P_{batt}}{V_{oc}C} \tag{5}$$

Here we assume that the optimal P_{batt} is a random variable. Define a variable $\mu = E(\frac{C_1 P_{batt}}{V_{oc}C})$ and a random variable $r = \frac{C_1 P_{batt}}{V_{oc}C} - \mu$. The above equation is re-written as:

$$\dot{\lambda} = -\lambda\mu - \lambda r \tag{6}$$

This is a stochastic first order differential equation. Since the distribution for r is unknown, it is hard to study this equation further. A preliminary assumption is that r has Gaussian distribution with zero mean. Then the above equation is rewritten as:

$$d\lambda = -\lambda\mu dt - \lambda r dt = -\lambda\mu dt - \lambda\sigma dw, \tag{7}$$

where w is a Brownian motion (Wiener Process) with Gaussian distribution and variance equal to time t. Here σ is the standard deviation of r. The solution to this equation using $Itô$'s calculus is [18]:

$$\lambda(t) = \lambda_0 e^{-\mu t - \frac{\sigma^2}{2}t} e^{\sigma w(t)} \tag{8}$$

And its expected value is:

$$E(\lambda(t)) = \lambda_0 e^{-\mu t} \tag{9}$$

The value of μ needs to be estimated. For a charge sustaining HEV, $\mu \approx 0$. Then co-state dynamics becomes:

$$\lambda(t) = \lambda_0 e^{-\frac{\sigma^2}{2}t} e^{\sigma w(t)} \tag{10}$$

Before we study how the co-state $\lambda(t)$ evolves as function of time, let's estimate a value for σ:

$$\sigma^2 = \text{var}(\frac{C_1 P_{batt}}{V_{oc} C}) = \frac{C_1^2}{C^2}\text{var}(\frac{P_{batt}}{V_{oc}}) = \frac{k^2 C_1^2}{C^2}\text{var}(I), \tag{11}$$

where I is the battery current and k is a constant representing the average of estimated discharging efficiency over charging efficiency; and $k \approx 1$ for a charge sustaining HEV. Observing the global optimal solution for the selected configuration at different driving cycles we found that $var(I)$ varies between 900 and 1600 for a charge sustaining HEV. Defining $I_\sigma = \sqrt{\text{var}(I)}$, we have:

$$\sigma = \frac{kC_1}{C}\sqrt{\text{var}(I)} \approx \frac{kC_1 I_\sigma}{C} \tag{12}$$

For the selected configuration, $k \approx 1$, $C_1 = 0.16$, $C = 21.5 \times 3600$, and $\sigma = 8.3 \times 10^{-5}$. Considering the simulation time $t \leq t_{max} = 3600s$, σ, $\sigma w(t)$, and $-\frac{\sigma^2}{2}t$ are small; therefore we can approximate $\lambda(t)$ in Eq. (10) as:

$$\lambda(t) \approx \lambda_0(1 - \frac{\sigma^2}{2}t)(1 + \sigma w(t)) \tag{13}$$

Consider the 95% confidence interval of $w(t)$ as $[-1.96\sqrt{t}, 1.96\sqrt{t}]$. This interval indicates that the probability of $|w(t)| < 1.96\sqrt{t}$ is 95%. Assume $w(t) = \pm 1.96\sqrt{\text{var}(w(t))} = \pm 1.96\sqrt{t}$. Then

$$\lambda(t) \approx \lambda_0(1 - \frac{\sigma^2}{2}t)(1 \pm 1.96\sigma\sqrt{t})$$

σ^2 is very small, thus the term $(1 - \frac{\sigma^2}{2}t)$ can be approximated as 1. Substituting the value of σ and with the simulation time of $t_f = t_{max} = 3600s$ we obtain:

$$\lambda(t_f) = \lambda_0(1 \pm 1.6 \times 10^{-4}\sqrt{t_f}) = \lambda_0(1 \pm 0.0096)$$

which indicates that for an HEV the difference between the final co-state $\lambda(t)$ and its initial guess is less than 0.96% with probability of 95% within the simulation time of 1 hour.

For a PHEV the following changes should be made,

$$\mu = E(\frac{C_1 P_{batt}}{V_{oc} C}) \approx \frac{C_1 k}{C} E(I) = \frac{C_1 k \mu_I}{C},$$

where $\mu_I = E(I)$. Using Eq. (9), we have:

$$E(\lambda(x_t)) = \lambda_0 e^{-\frac{C_1 k \mu_I t}{C}} = \lambda_0 e^{-C_1 k C_{x_t}},$$

where C_{x_t} is the discharge depth at position x_t and expressed as $C_{x_t} = \frac{\mu_I t}{C}$.

By the definition of the relation between co-state $\lambda(t)$ and equivalent factor s in Eq.3.10, at any position x_t, the average value of the equivalent factor $E(s(x_t))$ is expressed as:

$$E(s(x_t)) = -E(\frac{\lambda(x_t) H_f}{V_{oc}(x_t) C}) = -\frac{H_f}{V_{oc}(x_t) C} E(\lambda(x_t))$$

The value of $V_{oc}(x_t)$ can be solved using Eq. (3):

$$V_{oc}(x_t) = V_{oc}(0) e^{-C_1(SOC_0 - SOC)} = V_{oc}(0) e^{-C_1 C_{x_t}}$$

Then $E(s(x_t))$ is related to its initial value s_i by:

$$\begin{aligned} E(s(x_t)) &= -\frac{H_f}{V_{oc}(x_t) C} \lambda_0 e^{-C_1 k C_{x_t}} \\ &= -\frac{H_f \lambda_0}{V_{oc}(0) C} \frac{e^{-C_1 k C_{x_t}}}{e^{-C_1 C_{x_t}}} = s_i e^{(1-k) C_1 C_{x_t}} \end{aligned} \tag{14}$$

For the PHEV used in the simulation case studies of this part, the parameter $k \approx 0.96$. Thus the term $(1-k) C_1 C_{x_t}$ is very small and $E(s(x_t))$ is approximated by:

$$E(s(x_t)) \approx s_i(1 + (1-k) C_1 C_{x_t}) \approx s_i(1 + 0.0064 \times C_{x_t})$$

Considering the maximum discharge depth of $max(C_{x_t}) = 0.6$, the term $(1-k) C_1 C_{x_t}$ is also small.

Therefore we conclude that the average value of optimal equivalent factor does not vary much considering variation of V_{oc} along the whole trip with the selected PHEV configuration.